

# A Two-Phase Model of Early Atherosclerotic Plaque Development with LDL Toxicity Effects

Abdush Salam Pramanik<sup>a</sup>, Bibaswan Dey<sup>a,\*</sup>, G. P. Raja Sekhar<sup>b</sup>

<sup>a</sup>*Department of Mathematics, University of North Bengal, Raja Rammohunpur, Darjeeling-734013, West Bengal, India*

<sup>b</sup>*Department of Mathematics, Indian Institute of Technology Kharagpur, Kharagpur-721302, West Bengal, India*

---

## Abstract

Atherosclerosis is a chronic inflammatory cardiovascular disease in which fatty plaque is built inside an artery wall. Early atherosclerotic plaque development is typically characterised by inflammatory tissues primarily consisting of foam cells and macrophages. We present a multiphase model that explores early plaque growth to emphasise the role of cytokines (in particular, Monocyte Chemoattractant Protein-1) and oxidised low-density lipoprotein (oxLDL) in monocyte recruitment and foam cell production, respectively. The plaque boundary is assumed to move at the same speed as the inflammatory tissues close to the periphery. This study discusses oxLDL-induced toxic environment towards macrophages and foam cells such that they start to die beyond a threshold limit of oxLDL concentration owing to excessive consumption. Our findings reveal that initially, the plaque evolves rapidly, and the growth rate subsequently reduces because of oxLDL-induced toxicity. In addition, it is observed that the saturation of inflammatory cell volume fraction becomes independent of oxLDL concentration beyond the threshold limit, referred to as the oxLDL toxicity limit. Our study manifests that increased oxLDL flux promotes flattened plaque growth through oxLDL-induced toxicity, while elevated cytokines flux disrupts the corresponding flattened behaviour. Detailed analysis of the model presented in this article unfolds critical insights into the various biochemical and cellular mechanisms

---

\*Corresponding author

Email address: [bibaswande@nbu.ac.in](mailto:bibaswande@nbu.ac.in) (Bibaswan Dey)

behind early plaque development.

*Keywords:* Oxidised LDL (oxLDL), Functional Cytokines (f-cytokines), Macrophage, Foam Cell, Perturbation Approximation, Mixture Theory

---

## 1. Introduction

Atherosclerosis, a type of cardiovascular diseases (CVDs), is an inflammatory disease associated with an excess concentration of low-density lipoprotein (LDL) in the bloodstream. Primarily, atherosclerosis occurs within bifurcated large and medium arteries, particularly at the position of curvature where a low value of endothelium shear stress is anticipated (Chatzizisis et al., 2007). The atherosclerotic plaque formation begins with the deposition of sizeable lipid-laden foam cells derived from monocytes which ingest oxidized low-density lipoprotein (oxLDL) through phagocytosis present within intima (Libby et al., 2002). Plaque formation is almost asymptomatic in a patient with atherosclerosis unless diagnosed clinically (Davies and Woolf, 1993). Hence it is essential to detect the plaque at an early stage in order to prevent fatal health complications. Therefore, a complete understanding of plaque growth in early atherosclerosis is crucial.

Early atherosclerotic plaque develops in the narrow intimal layer of an artery. Fig. 1 depicts the layered structure of a healthy artery wall. When there is turbulence of recirculation in the blood flow into the lumen region, the endothelium gets damaged, particularly in areas of low shear stress. Several factors, such as hypertension, smoking, consuming processed foods and alcohol etc., expedite endothelium damage (Channon, 2006; Furchtgott, 1999). Low-density lipoprotein (LDL) from the bloodstream penetrates the artery wall to enter the intima through the injured endothelium, where free oxygen radicals modify LDL molecules to become oxidized LDL (oxLDL) (Lusis, 2000; Cobbold et al., 2002). In general, the secretion of monocyte chemoattractant protein-1 (MCP-1) can be coupled with the chemoattractant monocyte colony-stimulating factor (M-CSF) (Ibragimov et al., 2005; Filipovic et al., 2013) as oxLDL is one of the critical factors that is responsible for atherosclerosis. The presence of oxLDL enables endothelium cells to secrete MCP-1 and M-CSF (Wu et al., 2017). In addition, endothelial cells near oxLDL express leukocyte adhesion molecules such as vascular cell adhesion molecule-1 (VCAM-1) and intracellular adhesion molecules (ICAM-1), fa-

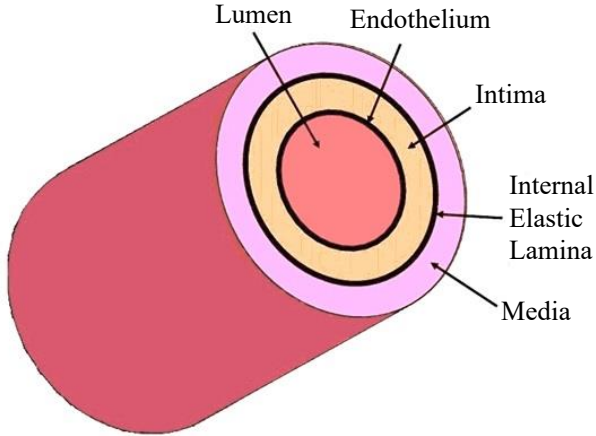


Figure 1: Cross-section of a healthy artery showing the artery wall consists of different cell layers. The innermost layer of the wall is comprised of a thin sheet of endothelium cells, called *the endothelium*. The endothelium forms an interface between the blood flow in the lumen and the rest of the artery wall. Immediately beneath the endothelium, a thin tissue layer lies called the *intima*. The underlying tissue layer is said to be *media* which is separated from the intima by a dense tissue membrane known as *internal elastic lamina (IEL)*.

cilitating monocyte attachment from the bloodstream (Lusis, 2000; Libby et al., 2002; Hansson and Libby, 2006). The monocytes enter the intima in response to chemoattractant gradients like MCP-1 and other cytokines (Han et al., 2004; Hansson and Libby, 2006; Lusis, 2000). Subsequently, monocytes differentiate into macrophages inside the intima in response to M-CSF (Ross, 1999; Libby et al., 2002). Macrophages within the intima consume oxLDL, which causes them to become large, lipid-laden foam cells (Lusis, 2000; Calvez et al., 2009; Gui et al., 2012; Hao and Friedman, 2014). Consequently, several foam cells produced with macrophages form an early plaque in atherosclerosis (Chalmers et al., 2015). At this early stage (early atherosclerosis), two essential components of the formed plaque are foam cells and macrophages. These foam cells further secrete more chemoattractants and cytokines to attract monocytes into the intima (Chalmers et al., 2017; Ross, 1999). Fig. 2 outlines the plaque formation at an early stage in a schematic diagram. In the later stage, smooth muscle cells (SMCs) migrate from the media to the intima through the IEL, induced by growth factors like platelet-derived growth factor (PDGF). Stimulated by transforming growth

factor-beta (TGF- $\beta$ ), SMCs produce collagen, with both migrated SMCs and collagen contributing to the formation of the fibrous cap near the endothelium (Newby and Zaltsman, 1999; Hansson et al., 2006). However, our focus is on early-stage plaque involving foam cells and macrophages, intending to develop a mathematical model that describes plaque growth and the corresponding biochemical mechanisms.

Although evidences on the death of macrophages and foam cells is not excessively available in the literature, some studies describe the possible cause. The toxic effect of cholesterol, mainly oxidized LDL, plays a significant role in macrophage or foam cell death. Feng et al. (2003); Zhang and Kaufman (2003) delve into the phenomenon of cholesterol-induced macrophage apoptosis, wherein cell death is linked to the depletion of calcium stores in the endoplasmic reticulum due to an excess of free cholesterol. According to Marchant et al. (1996); Gotoh et al. (1993), the toxic environment induced by oxLDL causes macrophages to die, starting after an initial lag phase, as demonstrated *in vitro* for human monocyte-macrophages. Excessive lipid ingestion can result in macrophage apoptosis, wherein macrophages undergo programmed cell death due to the high accumulation of lipids (Tabas et al., 2002; Watson et al., 2023). In addition, based on *in vitro* evidence of mulberry extracts on LDL oxidation and foam cell formation, Liu et al. (2008) demonstrated that macrophages could transform into foam cells when taking up low levels of oxLDL. However, at high oxLDL levels, macrophages lose their ability to process the same effectively, leading to cell death in both macrophages and foam cells. Consequently, a threshold value of oxLDL concentration exists, after which inflammatory cells (macrophages, foam cells) start to die (Liu et al., 2008). Note that the toxicity of oxLDL has been attributed to inflammatory cells without distinguishing between extracellular and intracellular environments, whether extracellular to macrophages or intracellular to foam cells. The dead foam cells within plaque release oxLDL and other cellular debris (Berliner et al., 1995). Macrophages consume more oxLDL and produce new foam cells.

Monocyte recruitment and differentiation have been studied using simplified mathematical modellings where the governing equations describe the conversion of macrophages into foam cells after consuming oxLDL with the involvement of various cytokines mentioned before (Calvez et al., 2009; Cohen et al., 2014; Chalmers et al., 2015). Ougrinovskaia et al. (2010) develops a simpli-

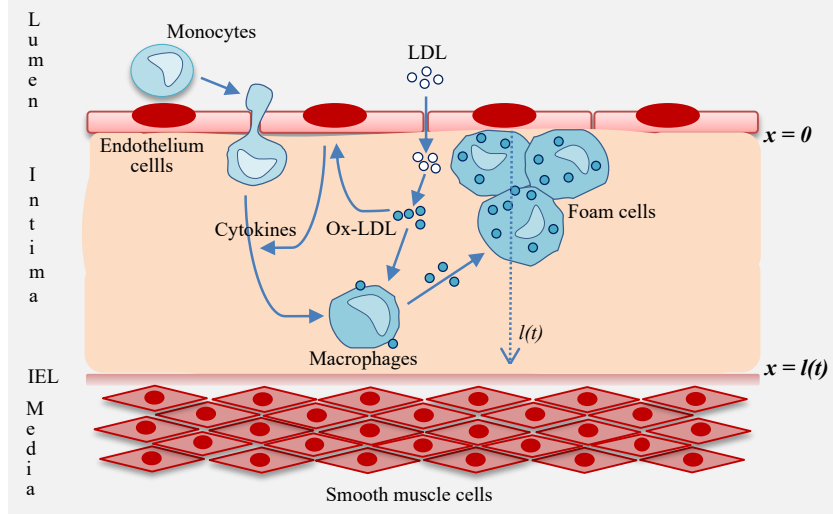


Figure 2: Schematic diagram of the key processes in plaque formation at the early stage. Low-density lipoprotein (LDL), which is present in the bloodstream, enters the intima through the damaged endothelium and undergoes modification to become oxidized LDL (oxLDL). OxLDL induces the secretion of several cytokines from the endothelium cells, including monocyte chemotactic protein-1 (MCP-1), monocyte colony-stimulating factor (M-CSF), and ES-cytokines. In response to the cytokines, particularly for MCP-1, monocytes adhere to the intima from the bloodstream and subsequently differentiate into macrophages. Within the intima, macrophages consume oxLDL to form large lipid-laden foam cells. The accumulation of foam cells produced by macrophages constitutes an early atherosclerotic plaque.

fied model at an early stage, including the uptake of oxLDL by macrophages to form foam cells. Their model assumes Michaelis-Menten kinetics for the uptake of oxLDL by macrophages, and the recruitment of macrophages depends on oxLDL. Moreover, they used a sigmoidal function to represent a saturated uptake rate. El Khatib et al. (2007, 2009, 2012) focus on plaque formation at an early stage of atherosclerosis where the density of monocytes and macrophages is represented as a system of reaction-diffusion equation. OxLDL draws monocytes or macrophages across the endothelium through nonlinear functions at the boundary. A similar but more extensive model for early plaque formation has been proposed by Calvez et al. (2009, 2010), which include macrophages and oxLDL and a cytokine produced in response to the consumption of oxLDL by macrophages and prompts the recruitment of the monocyte at the endothelium.

Atherosclerosis is a dynamical process of plaque growth that can be modelled using the Multiphase mixture theory (Breward et al., 2002; Byrne et al., 2003; Hubbard and Byrne, 2013; Dey and Raja Sekhar, 2016; Dey et al., 2018; Kumar et al., 2018; Alam et al., 2019; Pramanik et al., 2023). Multiphase models can produce a detailed description of plaque formation dynamics since they provide a natural framework for volume exclusion and mechanical interaction between plaque constituents. Recently Watson et al. (2018) have employed the mixture theory approach to model early fibrous cap formation and smooth muscle cells (SMCs) migration corresponding to the advanced stage of atherosclerosis plaque formation. Later, Watson et al. (2020) have considered an advanced plaque tissue, a mixture of three distinct phases: SMC phase, collagen-rich fibrous extracellular matrix (ECM) and a generic tissue phase comprising the remaining plaque constituents. Their study considers collagen cap formation by SMCs in response to diffusible growth factors like PDGF and TGF- $\beta$  from the endothelium. Most of the above studies consider the plaque material advanced and stable without apprising its overall growth. Consequently, the interface between the intima and media remains static. Hence, early plaque growth prediction through those models may be challenging. Many researchers believe that atherosclerosis is an obvious application of free boundary models, but for various reasons, most ignore it. In this context, the study of Ahmed et al. (2023) have introduced a free boundary multiphase model corresponding to early atherosclerotic plaques to investigate the effects of impaired macrophage anti-inflammatory behaviour on plaque structure and its growth. Motivated by the above developments of the atherosclerosis model, one can assume that the plaque boundary moves with a velocity equal to the speed of inflammatory tissue. Accordingly, in this study, we present a two-phase model in which plaques are formed by macrophages and foam cells through the uptake of oxLDL, characterized by a dynamic plaque boundary. Also, both the volume exclusion and mechanical interaction can be captured through the multiphase modelling which can play a crucial role in the plaque growth of early atherosclerosis. Our primary focus is to investigate the inflammatory response of macrophages and the impact of oxLDL-induced toxicity on plaque development. The multiphase approach of the atherosclerosis model and moving plaque boundary can capture critical chemo-mechanical features. In this context, modelling tumor domain having a free boundary could be a more realistic approximation of the scenario and certainly throws light on various aspects related to the tumor growth process (Breward et al., 2002; Byrne et al., 2003; Hubbard and Byrne, 2013).

This motivates us to investigate the model as a free boundary domain model.

This paper is structured through several sections. In the next section, we formulate a mathematical model based on the mixture theory, assuming atherosclerotic plaque as a two-phase material composed of inflammatory and non-inflammatory tissues. Further, governing equations for the plaque growth are simplified for a 1D cartesian geometry. The governing equations are nonlinear due to the underlying physics; however, the Michaelis–Menten general kinetics corresponding to the oxLDL metabolism by macrophages is highly significant. In order to linearize the oxLDL transport equation, a perturbation expansion method is deployed by assuming the weak nonlinear nature of the oxLDL metabolism. Subsequently, the finite difference method is applied to the resulting leading and first-order equations satisfying the CFL condition. The novel feature of this study is the use of a combination of perturbation and numerical methods for efficiently handling the nonlinearity related to the oxLDL metabolism by macrophages.

## 2. Mathematical Formulation

To model the growth of an early-stage atherosclerotic plaque, we hypothesize that it is caused by the accumulation of macrophages and foam cells. Indeed the conversion of monocytes into macrophages and rapid oxidization of LDL inside the intima take place on a much shorter time scale than the growth of the plaque (Chalmers et al., 2015). Tracking monocytes within the intima at any given moment would be challenging. Therefore, it is sufficient to view a monocyte as a macrophage and replace LDL with oxLDL. At this point, the plaque is comprised of two separate phases. One is made up of macrophages and foam cells, while the other includes interstitial fluid, oxLDL, cytokines, and more. The initial stage of atherosclerosis can be referred to as the inflammatory cell phase, as it predominantly involves macrophages and foam cells derived from macrophages in the development of the inflammatory disease. Therefore, the second phase is non-inflammatory. Inflammatory cells such as monocytes or macrophages migrate and infiltrate based on the regulation of MCP-1. This chemokine is activated by the endothelial cells and is a key player in the process. The inflammatory cell phase migration is caused by MCP-1 and other cytokines, also known as Endothelial Stimulating cytokines or ES cytokines. These cytokines can be considered as functional cytokines or f-cytokines. The transport of oxLDL and f-cytokines is represented by

standard transport reaction equations.

We assume that the domain of the plaque region is  $\Omega(t)$  in  $\mathbb{R}^d$  ( $d = 1, 2, 3$ ) with moving boundary  $\Gamma(t)$  that may be due to the several subparts. To begin, we will establish  $\Gamma_1$  as the portion of the plaque boundary related to the interface between the lumen and intima, or the endothelium. Then, we will define  $\Gamma_2(t)$  as the boundary of  $\Omega(t)$  that corresponds to the IEL. This boundary separates the intima from the media and increases in size over time due to the accumulation of macrophages and foam cells. Early plaque formation leads to compensatory expansion of an artery, during which the artery extends radially outward while preserving the lumen (Korshunov et al., 2007). Consequently, the intima-IEL boundary  $\Gamma_2(t)$  can be considered to vary over time. We introduce a finite index set  $\mathcal{C}$  containing the constituents of the plaque region. Based on our assumptions, the plaque is made up of two types of cells: inflammatory cells ( $f$ ) and non-inflammatory cells ( $n$ ), which we can denote as the set  $\mathcal{C} = \{f, n\}$ . Alternatively, we can represent it as  $\mathcal{C} = \{m, f, e\}$ , where  $m$  represents monocyte or macrophage,  $f$  stands for foam cell, and  $e$  denotes extracellular fluid matrix in the plaque region. For this study, we will focus on the two main constituents of the plaque: inflammatory and non-inflammatory cells, i.e.  $\mathcal{C} = \{f, n\}$ . However, it is also possible to consider a multiphase model.

### 2.1. *Mass Balance Equations*

We define  $\varphi^\alpha$  ( $\alpha \in \mathcal{C}$ ) as the volume fraction of each phase and  $\mathbf{v}^\alpha$  ( $\alpha \in \mathcal{C}$ ) as the velocity of each phase. Also, let us denote  $\mathbf{T}^\alpha$  ( $\alpha \in \mathcal{C}$ ) as the stress experienced by the  $\alpha$ -th phase. We assume that each phase has the same constant density. Mass balance equations corresponding to each phase can be expressed in the form

$$\frac{\partial \varphi^\alpha}{\partial t} + \nabla \cdot (\varphi^\alpha \mathbf{v}^\alpha) = \mathbf{\nabla}^\alpha, \quad (\alpha \in \mathcal{C}) \quad (1)$$

where  $\mathbf{v}^\alpha \in \mathbb{R}^d$  and  $\mathbf{\nabla}^\alpha \in \mathbb{R}$  is the net source term corresponding to the  $i$ -th phase. Since the plaque is formed by the constituent of  $\mathcal{C}$  and there are no voids, thus

$$\sum_{\alpha \in \mathcal{C}} \varphi^\alpha = 1. \quad (2)$$

The plaque growth model suggests that certain cells from bloodstream, such as monocytes or macrophages, can enter the intima (the innermost layer of

our arteries) through damaged parts of the endothelium (the inner lining of our blood vessels). These cells consume oxLDL, which is a type of cholesterol, and then transform into foam cells. Both macrophages and foam cells are involved in the inflammatory phase of plaque growth. Macrophages can accumulate large amounts of oxLDL, which can become toxic to foam cells (Hegyi et al., 1996). This toxic environment can also lead to macrophage death, resulting in the cellular debris becoming part of the non-inflammatory phase (Marchant et al., 1996). Assume that there is no local source or sink of material, and mass is transferred between these phases. Inflammatory cells take up material (oxLDL) from the non-inflammatory tissue phase and revert to the non-inflammatory phase upon their death. Therefore, the model is locally mass conservative and consequently satisfies the following:

$$\sum_{\alpha \in \mathcal{C}} \nabla^\alpha = 0. \quad (3)$$

## 2.2. Momentum Balance Equations

Under no external force and negligible inertial effect, the momentum balance equations reduce to the balance equations between intraphase and interphase forces for each inflammatory and non-inflammatory phase (Byrne et al., 2003; Hubbard and Byrne, 2013):

$$\nabla \cdot (\varphi^\alpha \mathbb{T}^\alpha) + \mathbf{\Pi}^\alpha = 0, \quad (\alpha \in \mathcal{C}) \quad (4)$$

where  $\mathbb{T}^\alpha \in \mathbb{R}^{d \times d}$  and  $\mathbf{\Pi}^\alpha \in \mathbb{R}^d$  is the interphase force exerted on the  $\alpha$ -th phase by the other phase. We assume the interphase force on the  $\alpha$ -th constituent from the Darcy law by the following relations (refer Breward et al. (2002, 2003); Hubbard and Byrne (2013))

$$\mathbf{\Pi}^\alpha = p \mathbb{I} \nabla \varphi^\alpha + \sum_{\beta \in \mathcal{C}}^{\beta \neq \alpha} \mathbf{K} \varphi^\alpha \varphi^\beta (\mathbf{v}^\beta - \mathbf{v}^\alpha) \quad (5)$$

in which,  $p \in \mathbb{R}$  is the hydrodynamic pressure of the interstitial fluid. The second term on the right-hand side in equation (5) represents the relative velocity between the phases characterized by a typical drag coefficient  $\mathbf{K} \in \mathbb{R}^{d \times d}$ .

### 2.3. Mass Transport Equations

OxLDL and f-cytokines present within the non-inflammatory phase are governed by the quasi-steady-state reaction-diffusion equations of the form

$$D_r \nabla \cdot (\varphi^n \nabla c_r) = Q_r, \quad r = \{1, 2\}, \quad (6)$$

in which  $c_1$  and  $c_2$  are concentrations of oxLDL and f-cytokines respectively.  $D_r \in \mathbb{R}$  denotes the diffusion coefficient and  $Q_r \in \mathbb{R}$  represents the net source or sink of the  $r$ -th species (Watson et al., 2018). Both  $Q_1$  and  $Q_2$  can be assumed to follow Michaelis-Menten kinetics. Since the characteristic timescale of diffusion for the above two species is significantly shorter than that of plaque growth, we neglect advective transport within the non-inflammatory phase and make a quasi-steady-state approximation (Hubbard and Byrne, 2013; Watson et al., 2020).

### 2.4. Stress Components

We propose the following constitutive relations corresponding to the stresses  $\mathbb{T}^\alpha$  ( $\alpha = n, f$ ) on the  $\alpha$ -th constituent present in equation (4) (Breward et al., 2003; Watson et al., 2018),

$$\mathbb{T}^f = - (p + \Sigma(\varphi^f) + \Lambda(c_2)) \mathbb{I}, \quad (7)$$

$$\mathbb{T}^n = -p \mathbb{I}, \quad (8)$$

where  $\Sigma : [0, 1] \rightarrow \mathbb{R}$  is a nonlinear function of the volume fraction of the inflammatory phase  $\varphi^f$ ;  $\Lambda : \mathbb{R} \rightarrow \mathbb{R}$  is another nonlinear function of the concentration of the f-cytokines  $c_2$ ;  $\mathbb{I}$  is the identity tensor. To simplify matters, we do not consider viscous forces on either phase, treating these phases as inviscid. As the growth process continues, the increased volume of the foam cells induces a cell-cell interaction. Therefore, beyond a specific value of  $\varphi^f$ , the membrane of each cell starts to deform, and the cells experience stress. In equation (7),  $\Sigma$  on the right-hand side represents the pressure during the inflammatory phase caused by cell-cell interactions. The migration of macrophages from the lumen to the intima is affected by f-cytokines. Therefore, the concentration of f-cytokines, denoted as  $c_2$ , controls the stress in the inflammatory phase. This concentration is expressed by the function  $\Lambda(c_2)$ .

### 2.5. Initial and Boundary conditions

The following initial and boundary conditions are required to complete the model.

### 2.5.1. Initial Conditions:

Both the inflammatory phase volume fraction and the plaque outer boundary  $\Gamma_2(t)$  are fixed initially:

$$\varphi^f(\mathbf{x}, 0) = \varphi_0^f, \quad \Gamma_2(t = 0) = \Gamma^0, \quad \text{for } \mathbf{x} \in \mathbb{R}^d. \quad (9)$$

### 2.5.2. Boundary Conditions:

The influx of LDL from the lumen into the intima occurs through the damaged portion of the endothelium. In the presence of free oxygen radicals inside the intima, LDL molecules oxidize to become oxLDL. The oxidation of LDL takes a much shorter time than plaque growth, as previously assumed. Consequently, both LDL influx and oxidation can be represented as a single process by the oxLDL influx. The flux of oxLDL through  $\Gamma_1$  is assumed to be constant and given by (Chalmers et al., 2015),

$$(\nabla c_1 \cdot \hat{n})|_{\Gamma_1} = -\nu_1, \quad (10)$$

where  $\hat{n}$  is the outward unit normal to the surface.

At the boundary  $\Gamma_1$ , the flux of f-cytokines is modelled by

$$(\nabla c_2 \cdot \hat{n})|_{\Gamma_1} = -\nu_2 c_1 - \nu_3 c_2. \quad (11)$$

Chemokines produced at the endothelium in response to oxLDL constitute a family of chemoattractant cytokines that play a significant role in selectively recruiting monocytes etc. (Lusis, 2000). MCP-1, like chemokines produced at the endothelium, recruit monocytes, and the incident is expressed by the first term on the right-hand side of the equation (11). ES cytokines enhance the production of MCP-1. As mentioned earlier, MCP-1, like chemokines and other ES cytokines, is regarded as f-cytokines. Therefore, in this context, it can be said that the production of f-cytokines by the endothelium depends on itself (Chalmers et al., 2015), which justifies the presence of the second term on the right-hand side of equation (11). Consequently, the flux of f-cytokines through the endothelium into the intima is influenced by the increasing concentrations of both oxLDL and f-cytokines at the endothelium (Hansson and Libby, 2006).

On the moving plaque boundary  $\Gamma_2(t)$ , we assume continuity of stress so that total stress of inflammatory and non-inflammatory cell phase balances the

stress of the outer media region, which is supposed to be constant. Accordingly, we set

$$(\mathbb{T}^f + \mathbb{T}^n) |_{\Gamma_2(t)} = \mathbb{T}^\infty. \quad (12)$$

We also assume that outside the plaque boundary  $\Gamma_2(t)$ , oxLDL and f-cytokines concentration are kept at constant sources, and thus we set

$$c_1 |_{\Gamma_2(t)} = c_1^\infty, \quad (13)$$

$$c_2 |_{\Gamma_2(t)} = c_2^\infty. \quad (14)$$

Finally, we assume that the plaque moving boundary  $\Gamma_2(t)$  expands at the same speed as the inflammatory cells on the boundary. Therefore, we define the following:

$$\frac{d\Gamma_2}{dt} = \mathbf{v}^f |_{\Gamma_2(t)}. \quad (15)$$

Here  $\mathbf{v}^f$  needs to be determined as part of the solution.

## 2.6. Constitutive Assumptions

### 2.6.1. Inflammatory Cell Phase Source Term

Macrophages migrate into the intima in response to f-cytokines. Experimental studies support the notion that f-cytokines, particularly MCP-1, stimulate macrophage proliferation during the progression of plaque formation (Zheng et al., 2016). Foam cells are produced when macrophages consume oxLDL, present in the non-inflammatory phase. Therefore, the production of inflammatory cells depends on the concentration of oxLDL ( $c_1$ ) and f-cytokines ( $c_2$ ). On the other hand, the primary cause of inflammatory cell death is oxLDL-induced toxicity due to the excess concentration of  $c_1$ . In addition to this, inflammatory cells undergo decay through natural cell death. Therefore, we choose  $\nabla^f$  by assuming both production and degradation or death saturating rates following Michaelis-Menten kinetics:

$$\nabla^f = \underbrace{\varphi^f \varphi^n \left( \frac{s_0 c_2}{1 + s_1 c_2} + \frac{s_2 c_1}{1 + s_3 c_1} \right)}_{\text{production}} - \underbrace{\varphi^f \left( \frac{s_4 + s_5 c_1}{1 + s_6 c_1} \right) \mathcal{H}(c_1 - c_1^*)}_{\text{death}} - \underbrace{\varphi^f s_7}_{\text{decay}}, \quad (16)$$

where the first two terms correspond to the production of inflammatory cells characterized by the parameters  $s_0$ ,  $s_1$ ,  $s_2$ , and  $s_3$ , and the third term represents the death of inflammatory cells characterized by  $s_4$ ,  $s_5$ , and  $s_6$ . The

production rate of inflammatory cells increases with  $c_1$  up to a fixed value  $c_1^*$  (can be referred to as oxLDL-induced reference toxicity level), beyond which oxLDL results in the death of inflammatory cells. In other words, beyond such  $c_1^*$ , the death rate of inflammatory cells increases with  $c_1$ . The last term denotes a marginal linear decay component corresponding to natural cell death.  $\mathcal{H}$  in equation (16) denotes the Heaviside function which can be approximated by a smooth function as (Hubbard and Byrne, 2013)

$$\mathcal{H}(x, \epsilon) = \frac{1}{2} \left\{ 1 + \tanh \left( \frac{x}{\epsilon} \right) \right\}, \quad \epsilon \ll 1. \quad (17)$$

### 2.6.2. OxLDL and f-Cytokines Source Terms

Net source or sink of oxLDL,  $Q_1$  can be assumed as follows

$$Q_1 = \underbrace{\varphi^f \varphi^n \left( \frac{q_0 c_1}{1 + q_1 c_1} \right)}_{\text{consumption}} - \underbrace{\varphi^f \varphi^n (q_2 c_1)}_{\text{release}}, \quad (18)$$

in which  $q_0$ ,  $q_1$  and  $q_2$  are positive constants. The first term on the right describes the loss of oxLDL due to the oxLDL consumption by macrophages to become foam cells. We use a Michaelis-Menten general kinetics type function to represent it. The oxLDL released by the dead foam cells are assumed to obey a constant decay rate (see the second term on the right-hand side of equation (18)) (Berliner et al., 1995). Note that there may be a loss of oxLDL, perhaps through degradation, but we do not include this for simplicity.

Similarly,  $Q_2$ , the net source or sink of f-cytokines can be set as

$$Q_2 = \underbrace{\varphi^n q_3 c_2}_{\text{decay}} - \underbrace{\varphi^n \varphi^f (q_4 c_1 c_2)}_{\text{production}}, \quad (19)$$

where  $q_3$  and  $q_4$  are positive constants. Cytokines secreted from foam cells in presence of oxLDL (Chalmers et al., 2017). Correspondingly, the production of f-cytokines depends on  $\varphi^f$  and  $c_1$ , as shown by the second term of the right hand side of above equation. The first term represents a linear decay in  $c_2$ .

### 2.6.3. Terms Contributing on Stress Tensor

The function  $\Sigma$  in equation (7) represents the pressure on inflammatory cell phase due to cell-cell interactions, which can be expressed as

$$\Sigma(\varphi^f) = \frac{(\varphi^f - \varphi^*)}{(1 - \varphi^f)^2} \mathcal{H}(\varphi^f - \varphi^*), \quad (20)$$

where  $\varphi^*$  is the volume fraction of foam cells and macrophages beyond which cells experience stress. Our choice of  $\Sigma$  follows the study of Breward et al. (2002); Byrne et al. (2003). f-Cytokines act as chemoattractants to pull monocytes from the lumen into the intima. It has already been mentioned that monocytes rapidly transform into macrophages inside the intima. Hence, the movement of macrophages within the intima can be assumed to be influenced by f-cytokines concentration (i.e. chemotaxis). Therefore,  $\Lambda$  in equation (7) can be defined to be

$$\Lambda = \frac{\chi}{1 + (\kappa c_2)^m}, \quad (21)$$

where  $\chi$ ,  $\kappa$  and  $m$  are positive parameters. The assumption implies that the stress from the inflammatory phase decreases with increasing f-cytokines concentration, allowing the chemoattractant to move. Correspondingly, it is represented as a mechanism of stress relief in the inflammatory cell phase (Watson et al., 2018). The chemotactic function  $\Lambda$  also can be defined as  $\chi/(1 + \kappa c_2)^2$ , but in the case of the receptor binding, it may be more reasonable to describe by Hill function as shown in (21) (Hillen and Painter, 2009). In this model, monocytes enter the intima from the bloodstream with the help of receptors VCAM-1 and ICAM-1. Consequently, our study would prefer to consider the chemotaxis function as (21).

## 3. 1D Model

As the first step, we study plaque growth in one dimension along the  $x$ -axis. It occupies the region  $0 \leq x \leq l(t)$  (see Fig. 2). Consequently, the boundary  $\Gamma_1$  reduces to  $x = 0$  (i.e., the interface of the endothelium and intima), and the moving edge  $\Gamma_2(t)$  corresponds to the interface of the intima. IEL is now  $x = l(t)$ , which is the width of the growing plaque at time  $t$  in the early stage. This one-dimensional model would enable us to focus on the cellular and biochemical mechanisms without worrying about the geometry of the

domain. Furthermore, the diameter of an artery is significantly larger than the width of the intima at the early stages of plaque formation (Bonithon-Kopp et al., 1996), which makes it reasonable to use Cartesian coordinates as an approximation for radial coordinates. We denote all the physical variables consistent with the previous section. The above scenario compels us to reduce the mass balance equations (1) into the following form:

$$\frac{\partial \varphi^f}{\partial t} + \frac{\partial}{\partial x} (\varphi^f v^f) = \nabla^f, \quad (22)$$

$$\frac{\partial \varphi^n}{\partial t} + \frac{\partial}{\partial x} (\varphi^n v^n) = \nabla^n. \quad (23)$$

Similarly, the momentum conservation equations (4) reduce as,

$$\frac{\partial}{\partial x} (\varphi^f T^f) + \Pi^f = 0, \quad (24)$$

$$\frac{\partial}{\partial x} (\varphi^n T^n) + \Pi^n = 0, \quad (25)$$

in which

$$\Pi^f = p \frac{\partial \varphi^f}{\partial x} + k \varphi^f \varphi^n (v^n - v^f) \quad (26)$$

and

$$\Pi^n = p \frac{\partial \varphi^n}{\partial x} + k \varphi^f \varphi^n (v^f - v^n), \quad (27)$$

as obtained from (5). The stresses described in equations (7) and (8) are reduced to the following 1D form

$$T^f = - (p + \Sigma (\varphi^f) + \Lambda(c_2)) \quad (28)$$

and

$$T^n = -p \quad (29)$$

respectively.

Next, the mass transport equations (6) reduce to

$$D_1 \frac{\partial}{\partial x} \left( \varphi^n \frac{\partial c_1}{\partial x} \right) = Q_1, \quad (30)$$

$$D_2 \frac{\partial}{\partial x} \left( \varphi^n \frac{\partial c_2}{\partial x} \right) = Q_2. \quad (31)$$

The reduction of boundary and initial conditions into 1D form is discussed in the next section, which focuses on simplifying the model.

### 3.1. Model Simplification

The entire model of early stage plaque growth is expressed into a system of nonlinear partial differential equations in  $\varphi^f$ ,  $v^f$ ,  $c_1$  and  $c_2$ . The simplification of this model follows the similar approach to that of Breward et al. (2002); Byrne and Preziosi (2003); Watson et al. (2018), and for clarity, the model simplification is included in detail. First we add the mass balance equations (22) and (23), to get

$$\frac{\partial}{\partial x} (\varphi^f v^f + \varphi^n v^n) = 0, \quad (32)$$

which upon integration results

$$(\varphi^f v^f + \varphi^n v^n) = v_0^{\text{com}}, \quad (33)$$

where the right hand side of the above equation stands for the composite velocity of the mixture at the endothelium-intima interface (EII). It is reasonable to impose  $v^n(0) = 0$  within  $v_0^{\text{com}}$  as the non-inflammatory phase cannot escape from the plaque. Hence,  $v_0^{\text{com}}$  becomes the product of inflammatory cell phase volume fraction and corresponding velocity at  $x = 0$ , which will be denoted as  $V_0$ . Consequently,  $v^n$  is expressed as follows

$$v^n = \left( \frac{V_0 - \varphi^f v^f}{\varphi^n} \right). \quad (34)$$

Apparently,  $V_0$  becomes the velocity of macrophages at  $x = 0$  with which they enter the intima under the influence of f-cytokines. Realistic value of  $V_0$  can be obtained from literature (according to van den Bos et al. (2020),  $V_0$  is of order  $1 \mu\text{m}/\text{min}$ ).

Now, summing the momentum balance equations (24) and (25), and submitting the stress expressions  $T^f$  and  $T^n$  from (28)-(29), we obtain

$$\frac{\partial p}{\partial x} + \frac{\partial F}{\partial x} = 0, \quad (35)$$

where

$$F = \varphi^f (\Sigma + \Lambda). \quad (36)$$

We derive the following from (35) with the help of (24), (26) and (28):

$$\varphi^n \frac{\partial F}{\partial x} + k (\varphi^f v^f - \varphi^f V_0) = 0. \quad (37)$$

Consequently, with the help of mass balance equation (22), we deduce

$$\frac{\partial \varphi^f}{\partial t} + V_0 \frac{\partial \varphi^f}{\partial x} - \frac{\varphi^n}{k} \left[ \frac{\partial^2 F}{\partial x^2} + \frac{1}{\varphi^n} \frac{\partial \varphi^n}{\partial x} \frac{\partial F}{\partial x} \right] = \nabla^f. \quad (38)$$

Now, from the equations (34) and (37) and employing the expression of  $F$  as provided in equation (36), we derive the following:

$$k(v^n - V_0) = \frac{\partial}{\partial x} (\varphi^f \Lambda) + \frac{\partial}{\partial x} (\varphi^f \Sigma). \quad (39)$$

Using the condition,  $v^n = 0$  at  $x = 0$ , we arrive at the following boundary condition

$$\frac{\partial}{\partial x} (\varphi^f \Lambda) + \frac{\partial}{\partial x} (\varphi^f \Sigma) + kV_0 = 0 \quad \text{at } x = 0, \quad (40)$$

which suggests the influx of inflammatory cells inside the intima via a chemo-tactic response to the f-cytokines at the endothelium-intima interface (EII).

The boundary conditions (10)-(11) reduce to 1D form as

$$D_1 \left( \frac{\partial c_1}{\partial x} \right) = -\nu_1, \quad \text{at } x = 0, \quad (41)$$

$$D_2 \left( \frac{\partial c_2}{\partial x} \right) = -\nu_2 c_1 - \nu_3 c_2, \quad \text{at } x = 0, \quad (42)$$

The stress boundary condition (12) reduce to

$$T^f + T^n = 1, \quad \text{at } x = l(t), \quad (43)$$

which further simplifies to at  $x = l(t)$ :

$$\Sigma(\varphi^f) + \Lambda(c_2) + (2p + 1) = 0. \quad (44)$$

At the plaque boundary  $x = l(t)$ , we assume the interstitial hydrodynamic pressure ( $p$ ) in such a way that  $2p + 1 = 0$ . We therefore have

$$\Sigma(\varphi^f) + \Lambda(c_2) = 0, \quad \text{at } x = l(t). \quad (45)$$

The boundary conditions (13) - (14) become

$$c_1 = c_1^\infty, \quad \text{at } x = l(t), \quad (46)$$

$$c_2 = c_2^\infty, \quad \text{at } x = l(t), \quad (47)$$

Furthermore, the boundary condition (15), describing the relationship between plaque width and velocity, reduces to

$$\frac{dl}{dt} = v^f. \quad \text{at } x = l(t). \quad (48)$$

Finally, we close the system by reducing the initial conditions (9) as

$$\varphi^f = \varphi_0^f, \quad l = l_0, \quad \text{at } t = 0, \quad (49)$$

Therefore, our reduced model can be read as the equation (30) coupled with equations (31), (37) and (38) subject to the boundary and initial conditions prescribed by (40)-(42), (45)-(48) and (49).

### 3.2. Nondimensionalization

Using hat ('^') to denote dimensionless quantities, we scale the independent and dependent variables  $x$ ,  $t$ ,  $l$ ,  $v^f$ ,  $c_1$ ,  $c_2$ ,  $\varphi^f$  and  $\varphi^n$ , as follows (one can note that, inflammatory and non-inflammatory cell phase volume fractions  $\varphi^f$  and  $\varphi^n$  respectively do not require scaling):

$$\hat{x} = x/l_0, \quad \hat{t} = t/(kl_0^2/T^\infty), \quad \hat{l} = l/l_0, \quad \hat{v}^f = v^f/(T^\infty/kl_0).$$

$$\hat{c}_1 = c_1/c_1^\infty, \quad \hat{c}_2 = c_2/c_2^\infty, \quad \hat{\varphi}^f = \varphi^f, \quad \hat{\varphi}^n = \varphi^n.$$

We introduced the non-dimensional parameters in the following way:

$$\hat{\mathbf{V}}^f = \mathbf{V}^f/(T^\infty/kl_0^2), \quad \hat{\Sigma} = \Sigma/T^\infty, \quad \hat{\Lambda} = \Lambda/T^\infty, \quad \hat{T}^f = T^f/T^\infty,$$

$$\hat{T}^n = T^n/T^\infty, \quad \hat{F} = F/T^\infty, \quad \hat{Q}_1 = Q_1/(D_1 c_1^\infty/l_0^2), \quad \hat{Q}_2 = Q_2/(D_2 c_2^\infty/l_0^2),$$

$$\hat{\nu}_1 = \nu_1/(D_1 c_1^\infty/l_0), \quad \hat{\nu}_2 = \nu_2/(D_2 c_2^\infty/l_0 c_1^\infty), \quad \hat{\nu}_3 = \nu_3/(1/l_0), \quad \hat{V}_0 = V_0/(T^\infty/kl_0).$$

The corresponding model equations, initial and boundary conditions in non-dimensional form reduce to

$$\frac{\partial \hat{\varphi}^f}{\partial \hat{t}} + \hat{V}_0 \frac{\partial \hat{\varphi}^f}{\partial \hat{x}} - \hat{\varphi}^n \frac{\partial^2 \hat{F}}{\partial \hat{x}^2} - \frac{\partial \hat{\varphi}^n}{\partial \hat{x}} \frac{\partial \hat{F}}{\partial \hat{x}} = \hat{\mathbf{V}}^f \quad (50)$$

$$\hat{\varphi}^n \frac{\partial \hat{F}}{\partial \hat{x}} + \hat{\varphi}^f \left( \hat{v}^f - \hat{V}_0 \right) = 0, \quad (51)$$

$$\frac{\partial}{\partial \hat{x}} \left( \hat{\varphi}^n \frac{\partial \hat{c}_1}{\partial \hat{x}} \right) = \hat{Q}_1, \quad (52)$$

$$\frac{\partial}{\partial \hat{x}} \left( \hat{\varphi}^n \frac{\partial \hat{c}_2}{\partial \hat{x}} \right) = \hat{Q}_2, \quad (53)$$

$$\hat{\varphi}^f = \varphi_0^f, \quad \hat{l} = 1, \quad \text{at } \hat{t} = 0, \quad (54)$$

$$\frac{\partial}{\partial \hat{x}} \left( \hat{\varphi}^f \hat{\Lambda} + \hat{\varphi}^f \hat{\Sigma} \right) + \hat{V}_0 = 0, \quad \text{at } \hat{x} = 0, \quad (55)$$

$$\frac{\partial \hat{c}_1}{\partial \hat{x}} = -\hat{\nu}_1, \quad \text{at } \hat{x} = 0, \quad (56)$$

$$\frac{\partial \hat{c}_2}{\partial \hat{x}} = -\hat{\nu}_2 \hat{c}_1 - \hat{\nu}_3 \hat{c}_2, \quad \text{at } \hat{x} = 0, \quad (57)$$

$$\hat{\Sigma}(\hat{\varphi}^f) + \hat{\Lambda}(\hat{c}_2) = 0, \quad \text{at } \hat{x} = \hat{l}(t), \quad (58)$$

$$\hat{c}_1 = 1, \quad \text{at } \hat{x} = \hat{l}(t), \quad (59)$$

$$\hat{c}_2 = 1, \quad \text{at } \hat{x} = \hat{l}(t), \quad (60)$$

and

$$\frac{d\hat{l}}{d\hat{t}} = \hat{v}^f. \quad \text{at } \hat{x} = \hat{l}(t). \quad (61)$$

Without loss of generality, we drop the hat ('^') from the model field equations, and initial and boundary conditions unless otherwise stated explicitly.

### 3.3. Change of Variables

In order to execute numerical solutions, it is convenient to map the moving domain onto a fixed one. Consequently, we change the variable  $(x, t)$  to  $(\zeta, \tau)$  by the transformation  $\zeta = x/l(t)$  and  $\tau = t$ . The transformed problem reduces to

$$\frac{\partial \varphi^f}{\partial \tau} - \left( \zeta \frac{dl}{d\tau} - \frac{V_0}{l} \right) \frac{\partial \varphi^f}{\partial \zeta} - \frac{\varphi^n}{l^2} \frac{\partial^2 F}{\partial \zeta^2} - \frac{1}{l^2} \frac{\partial \varphi^n}{\partial \zeta} \frac{\partial F}{\partial \zeta} = \nabla^f, \quad (62)$$

$$\varphi^n \frac{\partial F}{\partial \zeta} + l \varphi^f (v^f - V_0) = 0, \quad (63)$$

$$\frac{\partial}{\partial \zeta} \left( \varphi^n \frac{\partial c_1}{\partial \zeta} \right) = l^2 Q_1, \quad (64)$$

$$\frac{\partial}{\partial \zeta} \left( \varphi^n \frac{\partial c_2}{\partial \zeta} \right) = l^2 Q_2, \quad (65)$$

with initial and boundary conditions

$$\varphi^f = \varphi_0^f, \quad l = 1, \quad \text{at } \tau = 0 \quad (66)$$

$$\frac{\partial}{\partial \zeta} (\varphi^f \Lambda) + \frac{\partial}{\partial \zeta} (\varphi^f \Sigma) + l V_0 = 0, \quad \text{at } \zeta = 0, \quad (67)$$

$$\frac{\partial c_1}{\partial \zeta} = -l \nu_1, \quad \text{at } \zeta = 0, \quad (68)$$

$$\frac{\partial c_2}{\partial \zeta} = -l \nu_2 c_1 - l \nu_3 c_2, \quad \text{at } \zeta = 0, \quad (69)$$

$$\Sigma(\varphi^f) + \Lambda(c_2) = 0, \quad \text{at } \zeta = 1, \quad (70)$$

$$c_1 = 1, \quad \text{at } \zeta = 1, \quad (71)$$

$$c_2 = 1, \quad \text{at } \zeta = 1, \quad (72)$$

and

$$\frac{dl}{d\tau} = v^f \quad \text{at } \zeta = 1. \quad (73)$$

#### 4. Computational Technique

A stable finite difference scheme for the numerical solution of the governing equations is employed. Specifically, explicit finite difference methods are applied to solve parabolic-type partial differential equations. The present differential nonlinear system is parabolic and amenable to using explicit finite-difference formulation. To solve the problem, we utilized the explicit finite-difference scheme known as the forward-time central space (FTCS) method, following the approach outlined in the studies by Zaman et al. (2016); Lee et al. (2013). One can refer to the book by Hoffmann and Chiang (2000) for comprehensive details of the method. This scheme approximates spatial derivatives by central difference formulae, while the forward difference formula approximates the time derivative.

We discrete the region  $(0,1)$  into  $N$  equal cells of size  $\Delta \zeta = 1/N + 1$  with a time step  $\Delta \tau > 0$ . Define  $\zeta_j = (j - 1)\Delta \zeta$ ,  $j = 1, 2, \dots, N + 1$ , and  $\tau_n = (n - 1)\Delta \tau$ ,  $n = 1, 2, \dots$ , and approximations  $[\varphi^f]_j^n = \varphi^f(\zeta_j, \tau_n)$ ,  $[c_1]_j^n = c_1(\zeta_j, \tau_n)$ ,

and  $[c_2]_j^n = c_2(\zeta_j, \tau_n)$ . Spatial and time derivative approximations are as follows:

$$\frac{\partial c_\ell}{\partial \zeta} \cong \frac{[c_\ell]_{j+1}^n - [c_\ell]_{j-1}^n}{2\Delta\zeta}, \quad \ell = 1, 2 \quad (74)$$

$$\frac{\partial^2 c_\ell}{\partial \zeta^2} \cong \frac{[c_\ell]_{j+1}^n - 2[c_\ell]_j^n + [c_\ell]_{j-1}^n}{(\Delta\zeta)^2}, \quad \ell = 1, 2 \quad (75)$$

$$\frac{\partial \varphi^f}{\partial \zeta} \cong \frac{[\varphi^f]_{j+1}^n - [\varphi^f]_{j-1}^n}{2\Delta\zeta}, \quad (76)$$

$$\frac{\partial^2 \varphi^f}{\partial \zeta^2} \cong \frac{[\varphi^f]_{j+1}^n - 2[\varphi^f]_j^n + [\varphi^f]_{j-1}^n}{(\Delta\zeta)^2}, \quad (77)$$

and

$$\frac{\partial \varphi^f}{\partial \tau} \cong \frac{[\varphi^f]_j^{n+1} - [\varphi^f]_j^n}{\Delta\tau}. \quad (78)$$

The system (62)-(73) is discretized based on the approximations (74)-(78) and solved. We start with a given  $[\varphi^f]_j^n$  to compute  $[c_1]_j^n$ ,  $[c_2]_j^n$  using which  $[\varphi^f]_j^{n+1}$  is evaluated. To meet the CFL condition of the explicit scheme and achieve an accuracy of approximately  $10^{-7}$ , we took  $N = 30$  spatial steps and  $10^5$  time steps, ensuring the stability of the corresponding method through the CFL condition.

In equation (64), the term  $Q_1$  is nonlinear in  $c_1$ . Applying the central difference formula (74)-(75) in (64), a system of nonlinear equations in  $[c_1]_1^n$ ,  $[c_1]_2^n, \dots, [c_1]_{N+1}^n$  when  $q_1 \neq 0$  is obtained. Newton's method can solve this nonlinear system, which is a tedious job requiring high numerical programming skills. As a result, some studies assume  $q_1 = 0$  to remove the nonlinearity (Breward et al., 2002; Lee et al., 2013). But, this restricts the general kinetics and reduces it to first-order kinetics, a particular case of Michaelis–Menten kinetics. In the present study, we deal with the general kinetics and consider  $q_1$  as a small parameter ( $q_1 \ll 1$ ) so that it becomes a perturbation parameter rather than taking the vanishing limit. Therefore, we reduce the nonlinear form of  $Q_1$  in the variable  $c_1$  to a weakly linearized form using perturbation approximation with the perturbed parameter  $q_1$  as described in the following section.

#### 4.1. Perturbation Approximations

We consider the following perturbation approximations

$$c_\ell = c_\ell^{(0)} + q_1 c_\ell^{(1)} + \mathcal{O}(q_1^2), \quad \ell = 1, 2 \quad (79)$$

$$\varphi^f = (\varphi^f)^{(0)} + q_1 (\varphi^f)^{(1)} + \mathcal{O}(q_1^2), \quad (80)$$

$$v^f = (v^f)^{(0)} + q_1 (v^f)^{(1)} + \mathcal{O}(q_1^2). \quad (81)$$

Using the above approximations, we can get the following expansions

$$\varphi^n = (\varphi^n)^{(0)} + q_1 (\varphi^n)^{(1)} + \mathcal{O}(q_1^2), \quad (82)$$

$$\nabla^f = \nabla^{f(0)} + q_1 \nabla^{f(1)} + \mathcal{O}(q_1^2), \quad (83)$$

$$\Sigma = \Sigma^{(0)} + q_1 \Sigma^{(1)} + \mathcal{O}(q_1^2), \quad (84)$$

$$\Lambda = \Lambda^{(0)} + q_1 \Lambda^{(1)} + \mathcal{O}(q_1^2), \quad (85)$$

$$F = F^{(0)} + q_1 F^{(1)} + \mathcal{O}(q_1^2), \quad (86)$$

and

$$Q_\ell = Q_\ell^{(0)} + q_1 Q_\ell^{(1)} + \mathcal{O}(q_1^2), \quad \ell = 1, 2 \quad (87)$$

where the expressions of  $(\varphi^n)^{(0)}$ ,  $(\varphi^n)^{(1)}$ ,  $\nabla^{f(0)}$ ,  $\nabla^{f(1)}$ ,  $\Sigma^{(0)}$ ,  $\Sigma^{(1)}$ ,  $\Lambda^{(0)}$ ,  $\Lambda^{(1)}$ ,  $F^{(0)}$ ,  $F^{(1)}$ ,  $Q_1^{(0)}$ ,  $Q_1^{(1)}$ ,  $Q_2^{(0)}$ , and  $Q_2^{(1)}$  are described in the Appendix A and B. Correspondingly, the leading and  $\mathcal{O}(q_1)$  problems reduce as shown in the following sections.

##### 4.1.1. The Leading Order Problem

The governing equations and the initial and boundary conditions corresponding to the leading order problem reduce as shown in Table 1.

##### 4.1.2. The $\mathcal{O}(q_1)$ Problem

In the first order, the governing equations and the initial and boundary conditions reduce as shown in Table 2.

Now, the terms  $Q_1^{(0)}$  and  $Q_1^{(1)}$  are both linear in  $c_1^{(0)}$  and  $c_1^{(1)}$  respectively (see Appendix A & B). Therefore, in order to compute  $c_1^{(0)}$  and  $c_1^{(1)}$  numerically from the equations in Table 1 and 2 (specifically, the third governing equations from both tables), we can apply central difference formulae (74)-(75). Correspondingly, we will get a system of linear equations for each case which can be solved using the Thomas algorithm. Then we compute  $c_2^{(0)}$ ,  $c_2^{(1)}$  in

Table 1: Governing equations, along with initial and boundary conditions related to the leading order problem.

<u>Governing Equations</u>
$\frac{\partial(\varphi^f)^{(0)}}{\partial\tau} - \left(\frac{\zeta}{l}\frac{dl}{d\tau} - \frac{V_0}{l}\right)\frac{\partial(\varphi^f)^{(0)}}{\partial\zeta} - \frac{(\varphi^f)^{(0)}}{l^2}\frac{\partial^2 F^{(0)}}{\partial\zeta^2} - \frac{1}{l^2}\frac{\partial(\varphi^n)^{(0)}}{\partial\zeta}\frac{\partial F^{(0)}}{\partial\zeta} = \mathbf{T}^{f(0)},$
$(\varphi^n)^{(0)}\frac{\partial F^{(0)}}{\partial\zeta} + l(\varphi^f)^{(0)}(v^f)^{(0)} = lV_0,$
$\frac{\partial}{\partial\zeta}\left((\varphi^n)^{(0)}\frac{\partial c_1^{(0)}}{\partial\zeta}\right) = l^2 Q_1^{(0)},$
$\frac{\partial}{\partial\zeta}\left((\varphi^n)^{(0)}\frac{\partial c_2^{(0)}}{\partial\zeta}\right) = l^2 Q_2^{(0)},$
<u>Initial Conditions</u>
$(\varphi^f)^{(0)} = \varphi_0^f, \quad l = 1, \quad \text{at } \tau = 0,$
<u>Boundary Conditions</u>
$\frac{\partial}{\partial\zeta}\left[(\varphi^f)^{(0)}(\Lambda^{(0)} + \Sigma^{(0)})\right] = 0, \quad \text{at } \zeta = 0,$
$\frac{\partial c_1^{(0)}}{\partial\zeta} = -l\nu_1, \quad \text{at } \zeta = 0,$
$\frac{\partial c_2^{(0)}}{\partial\zeta} = -l\nu_2 c_1^{(0)} - l\nu_3 c_2^{(0)}, \quad \text{at } \zeta = 0,$
$\Sigma^{(0)}\left((\varphi^f)^{(0)}\right) + \Lambda^{(0)}\left(c_2^{(0)}\right) = 0, \quad \text{at } \zeta = 1,$
$c_1^{(0)} = 1, \quad \text{at } \zeta = 1,$
$c_2^{(0)} = 1, \quad \text{at } \zeta = 1,$
$\frac{dl}{d\tau} = (v^f)^{(0)} \quad \text{at } \zeta = 1.$

Table 2: Governing equations, along with initial and boundary conditions corresponding to the  $\mathcal{O}(q_1)$  problem.

<u>Governing Equations</u>	
$\frac{\partial(\varphi^f)^{(1)}}{\partial\tau} - \left(\frac{\zeta}{l}\frac{dl}{d\tau} - \frac{V_0}{l}\right)\frac{\partial(\varphi^f)^{(1)}}{\partial\zeta} - \frac{(\varphi^n)^{(0)}\frac{\partial^2 F^{(1)}}{\partial\zeta^2}}{l^2} - \frac{(\varphi^n)^{(1)}\frac{\partial^2 F^{(0)}}{\partial\zeta^2}}{l^2} - \frac{1}{l^2}\frac{\partial(\varphi^n)^{(0)}}{\partial\zeta}\frac{\partial F^{(1)}}{\partial\zeta} - \frac{1}{l^2}\frac{\partial(\varphi^n)^{(1)}}{\partial\zeta}\frac{\partial F^{(0)}}{\partial\zeta} = \nabla f^{(1)},$	
$(\varphi^n)^{(0)}\frac{\partial F^{(1)}}{\partial\zeta} + (\varphi^n)^{(1)}\frac{\partial F^{(0)}}{\partial\zeta} + l(\varphi^f)^{(0)}(v^f)^{(1)} + l(\varphi^f)^{(1)}\left((v^f)^{(0)} - V_0\right) = 0,$	
<u>Initial Conditions</u>	
$(\varphi^f)^{(1)} = 0, \quad l = 1, \quad \text{at } \tau = 0,$	
<u>Boundary Conditions</u>	
$\frac{\partial}{\partial\zeta}\left((\varphi^f)^{(0)}\Lambda^{(1)} + (\varphi^f)^{(1)}\Lambda^{(0)}\right) + \frac{\partial}{\partial\zeta}\left((\varphi^f)^{(0)}\Sigma^{(1)} + (\varphi^f)^{(1)}\Sigma^{(0)}\right) = 0, \quad \text{at } \zeta = 0,$	
$\frac{\partial c_1^{(1)}}{\partial\zeta} = 0, \quad \text{at } \zeta = 0,$	
$\frac{\partial c_2^{(1)}}{\partial\zeta} = -l\nu_2 c_1^{(1)} - l\nu_3 c_2^{(1)}, \quad \text{at } \zeta = 0,$	
$\Sigma^{(1)} + \Lambda^{(1)} = 0, \quad \text{at } \zeta = 1,$	
$c_1^{(1)} = 0, \quad \text{at } \zeta = 1,$	
$c_2^{(1)} = 0. \quad \text{at } \zeta = 1.$	

a similar way and finally we evaluate  $(\varphi^n)^{(0)}$  and  $(\varphi^n)^{(1)}$ . Consequently, we numerically obtain the solution of the leading and  $\mathcal{O}(q_1)$  problem. Hence, the complete solution is determined upto  $\mathcal{O}(q_1)$  from the equations (79)-(81).

## 5. Numerical Simulations

In this section, we systematically analyze the numerical results on the oxidized LDL concentration, volume of inflammatory phase (foam cells + macrophages), concentration of f-cytokines responsible for macrophage migration, the variation of plaque width over time, etc. First, we set the values of parameters of interest. Subsequently, numerical simulations are performed.

### 5.1. *Model Parameterisations*

The development of plaque in atherosclerosis occurs gradually over time. In vivo investigations carried out on rabbits and ApoE-/- or Ldlr-/- mice have demonstrated that the onset of atherosclerotic plaque formation occurs over a period of several days, ranging between 30 and 90 days (Badimon et al., 1990; Tangirala et al., 1999). Hence, in the present study of early plaque development, the time scale for the simulation is considered in days. The clinical study of Grootaert et al. (2015) mentions an average intimal thickness as  $75\mu\text{m}$  in the thoracic aorta of an ApoE-/- mice fed a high-fat diet for 10 or 14 weeks. Since the early plaque growth is restricted within the intima, one can choose the initial plaque width as  $l_0 = 10^{-2} \text{ cm}$ . As ApoE-/- mice have been found to more closely resemble the human metabolite signature of increased carotid intima-media thickness than other animal models of cardiovascular disease (Saulnier-Blache et al., 2018), the choice of  $l_0$  is relevant to human atherosclerosis as well. According to Hao et al. (2014), Hao and Friedman (2014), the diffusion coefficients for oxidized LDL and f-cytokines (in particular for MCP-1) are  $29.89 \text{ cm}^2\text{day}^{-1}$  and  $17.28 \text{ cm}^2\text{day}^{-1}$  respectively.  $q_0$  represents the rate of metabolism of oxidized LDL by macrophages, which is  $10^4 \text{ day}^{-1}$  (McKay et al., 2005). Similarly, the study of Cobbold et al. (2002) suggests the value of  $q_2$  (the rate of oxLDL production) as  $2.35 \times 10^{-7} \text{ day}^{-1}$ . In addition, Hao and Friedman (2014) and Chen et al. (2012) respectively support the production and decay rates of f-cytokines (i.e.,  $q_4$  and  $q_3$ ) as  $0.96 \times 10^{10} \text{ g}^{-1}\text{cm}^3\text{day}^{-1}$  and  $1.73 \text{ day}^{-1}$ . As reported by Hao and Friedman (2014), within the intima, the concentration of oxLDL and f-cytokines are  $7 \times 10^{-4} - 1.9 \times 10^{-3} \text{ gcm}^{-3}$  and  $3 \times 10^{-10} \text{ gcm}^{-3}$  respectively. The chemotactic sensitivity parameter  $\chi$ , as mentioned in equation (21) can

be set as  $15.5 \times 10^{-16} \text{ gcm}^{-1}\text{day}^{-2}$  (Kim and Friedman, 2010). With the data set mentioned above, we calculate the corresponding non-dimensional values of the parameters  $q_0, q_2, q_3, q_4$  and  $\chi$  as listed in Table 3. Note that we select the value of  $q_1$  consistent with the dimensionless value of  $q_0$ . In addition, this table contains the calculated dimensionless values of constants  $\nu_1, \nu_2$  and  $\nu_3$  that are present in equations (68)-(69) from the studies of Chalmers et al. (2015); Ougrinovskaia et al. (2010).

Table 3: Calculated dimensionless values of the parameters from the mentioned literatures.

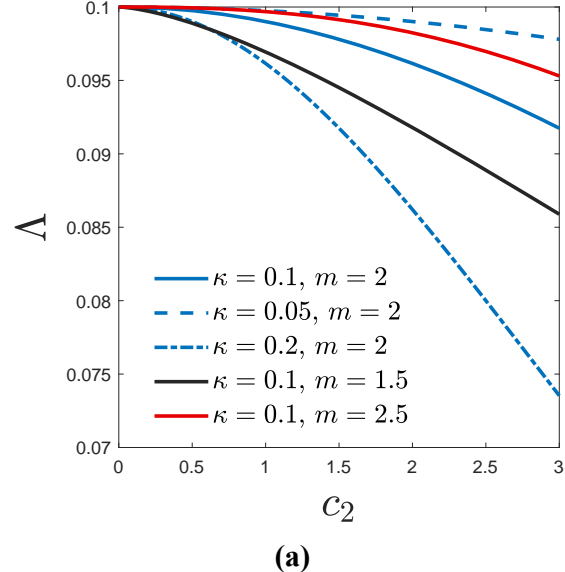
Parameter	Dimensionless value	Supporting literature
$q_0$	$3.3 \times 10^{-1}$	McKay et al. (2005)
$q_1$	$10^{-2}$	—
$q_2$	$7.8 \times 10^{-14}$	Cobbold et al. (2002)
$q_3$	$1 \times 10^{-6}$	Chen et al. (2012)
$q_4$	$5 \times 10^{-1}$	Hao and Friedman (2014)
$\chi$	$1 \times 10^{-1}$	Kim and Friedman (2010)
$\kappa$	$1 \times 10^{-1}$	—
$m$	2	—
$l_0$	$10^{-2}$	Grootaert et al. (2015)
$V_0$	$10^{-3}$	van den Bos et al. (2020)
$\nu_1$	$10^{-2} - 10^1$	Chalmers et al. (2015)
$\nu_2$	$10^{-2} - 10^1$	Ougrinovskaia et al. (2010)
$\nu_3$	$10^{-3} - 10^1$	Chalmers et al. (2015)

It has been noted that there is a need for more literature to accurately determine the values of the non-dimensional parameters  $\kappa$  and  $m$  in the chemotactic function  $\Lambda$ . As a result, suitable estimates for these parameters would be much handy. In this regard, the behaviour of  $\Lambda$  against  $c_2$  is shown in Fig. 3a to estimate  $\kappa$  and  $m$ . Following Hillen and Painter (2009), the estimates of these parameters can be selected within the ranges of  $0 < \kappa < 1$  and  $1 < m < 3$ . The chemotactic function generally has a decreasing nature corresponding to all values within the ranges, as shown in Fig. 3a.  $\Lambda$  is plotted for three different values of  $\kappa = 0.05, 0.1, 0.2$  and  $m = 1.5, 2, 2.5$ . It is also that for higher values of  $\kappa$ , the chemotactic function decays faster; however, this decay is slow for large  $m$ . Therefore,  $\kappa = 0.1$  and  $m = 2$  could be a worthy choice.

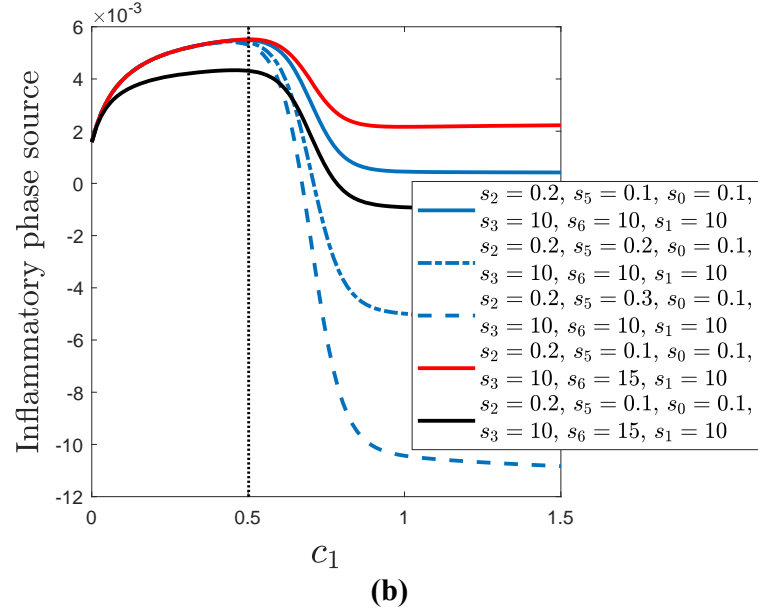
Table 4: Estimated values of the non-dimensional parameters contributing in inflammatory phase source term.

Parameter	Value
$s_0$	$10^{-1}$
$s_1$	10
$s_2$	$2 \times 10^{-1}$
$s_3$	10
$s_4$	$10^{-3}$
$s_5$	$10^{-1}$
$s_6$	10
$s_7$	$10^{-3}$

Similarly, we go through the behaviour of the inflammatory phase net source  $\nabla^f$  that appears in equation (16) to estimate the value of the parameters  $s_0, s_1, s_2, s_3, s_4, s_5$  and  $s_6$  (as shown in Fig. 3b). The parameters  $s_0$  and  $s_1$  are decided inversely proportional to each other, ensuring that the first term (in the production part) of  $\nabla^f$ , which increases with  $c_2$ , adequately represents the growth of the inflammatory phase. Likewise,  $s_2$  and  $s_3$  are selected to be inversely proportional to each other so that the second term (in the production part) of  $\nabla^f$  with the growth associated with  $c_1$ , thereby justifying the observed inflammatory phase development. We consider that the death of the inflammatory phase occurs due to the toxicity of oxLDL, where  $c_1^*$  is the reference toxicity level. Consequently, the contribution of the death term (i.e. second part in  $\nabla^f$ ) in the inflammatory cell production increases with  $c_1$  for values higher than  $c_1^*$ . Therefore, throughout the study,  $s_4 < s_5/s_6$  can be assumed. In addition,  $s_5$  and  $s_6$  may behave inversely towards the increasing nature of the death term. Hence upon the choice of  $s_6$  within [1, 10], it may be suitable to consider  $s_5$  in [0.1, 1] with the assumption  $s_4 < s_5/s_6$ . Also, the literature suggests that when  $s_1 = s_3 = s_6 = 0$  (first-order kinetics), the parameters  $s_0, s_2$  and  $s_5$  lies in the range  $0.1 \leq s_0, s_3 \leq 10$  (Prakash et al., 2010; Dey and Raja Sekhar, 2016). To adjust the parameter values within the specified ranges, we can consult Fig. 3b. Note that the net source term becomes negative when  $s_0, s_2 \leq s_5$ , as shown by the blue and dash-dotted lines. This incident may be physically unrealistic as the inflammatory phase forms the plaque. Hence, we can consider  $s_2 > s_5$ ,  $s_0 = s_5$  with  $s_2 = 0.2$ ,  $s_5 = 0.1$ , and  $s_0 = 0.1$ . In addition, in each of the following cases,  $s_3 < s_6$ ,  $s_3 = s_6$  and  $s_3 > s_6$ , the corresponding scenarios are shown by the solid



(a)



(b)

Figure 3: Variation of (a) chemotactic function  $\Lambda$  (21) with respect to  $c_2$ , (b) inflammatory phase source  $\nabla^f$  (16) with  $c_1$  corresponding to various parameters described in the figures.

red, blue and black curves, respectively. Similar arguments are valid for the

case  $s_3 \leq s_6$ . For simplicity, we choose  $s_3 = s_6 = 10$  following the study of Breward et al. (2002) on tumor growth, and  $s_1 = 10$ , consistent with those for  $s_3$  and  $s_6$ . The value of the parameter  $s_4$  is considered as  $10^{-3}$  to satisfy the condition  $s_4 < s_5/s_6$ . Finally, we select the value of the marginal decay parameter  $s_7$  as  $10^{-3}$  to align with the order of magnitude of the death term caused by toxicity. The above-estimated parameter values are prescribed in Table 4.

### 5.2. Results and Discussion

This section discusses the role of the inflammatory cell phase, oxLDL, f-cytokines, and non-inflammatory phase in plaque growth. It provides a thorough analysis of the overall impact of three parameters, namely  $\nu_1$ ,  $\nu_2$ , and  $\nu_3$ , on the inflammatory changes that occur in early atherosclerosis and the corresponding growth and contraction on plaque development. It is worth noting that the inflammatory cell phase predominantly contributes to early plaque expansion. In Fig. 4a, we observe how the volume of inflammatory cell phase changes over time at different locations within a growing plaque. The timeline ranges from  $t_{\text{fix}} = 10$  to  $t_{\text{fix}} = 35$  and the parameters used are  $\varphi_0^f = 0.6$ ,  $\varphi^* = 0.4$ , and  $c_1^* = 0.5$ , along with other parameters selected from Tables 3 and 4. The reason for choosing the above range for the timeline is significant and will be emphasized later. The values of  $\varphi_0^f$  and  $\varphi^*$  are initially chosen to include cell-cell interactions and continue with these values unless otherwise specified. The volume of the inflammatory cell population is found to be highest at the EII (i.e.  $x = 0$ ). Inflammatory cells accumulate mostly towards  $x = 0$ , and their volume decreases towards the moving medial boundary (or IEL boundary), i.e.,  $x = l(t)$ . Note that inflammatory cells are recruited through  $x = 0$ , resulting in a large amount of the inflammatory cells at that location. In due course of time, inflammatory cells gradually increase within the intima (see Fig. 4a). On the other hand, both oxLDL and f-cytokines are highly concentrated at the endothelium where they are secreted, and their concentration decreases while moving away from it (to affirm this, see the respective Fig. 4b-4c). As macrophages consume oxLDL and transform into foam cells, the number of inflammatory cells increases, causing a decrease in the concentration of oxLDL over time. However, as depicted in Fig. 4c, the concentration of f-cytokines tends to rise over time due to the secretion of these cytokines by inflammatory cells.

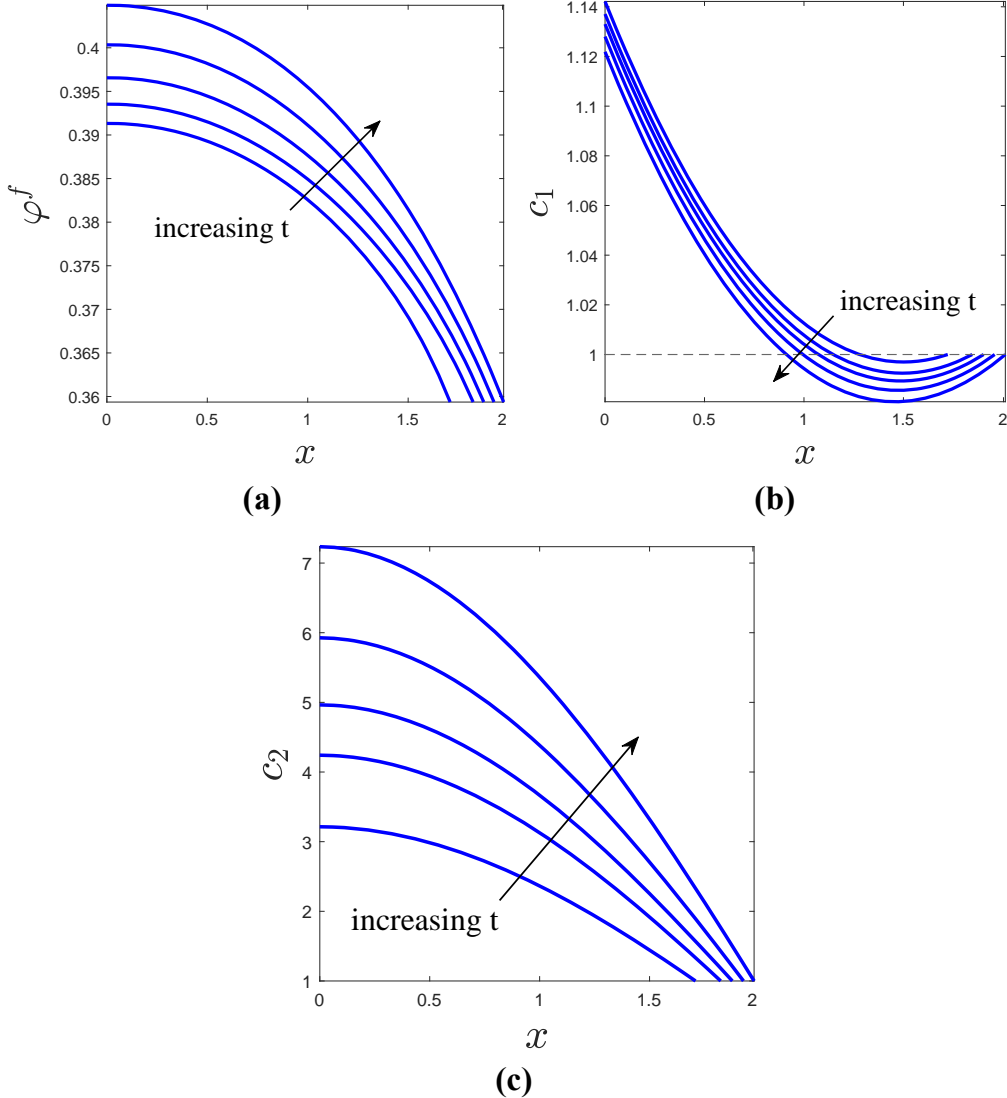


Figure 4: (a) Volumetric variation of inflammatory cells, (b) OxLDL concentration, and (c) f-Cytokines (MCP-1) concentration at every locations within plaque for various  $t_{\text{fix}} = 10, 20, 25, 30$  and  $35$  at an early stage of atherosclerosis. The direction of these sequential time points is indicated by the arrows.

Evidently,  $\varphi^f$ ,  $c_1$ , and  $c_2$  are mutually dependent. In the intima, macrophages consume oxLDL to become lipid-laden foam cells, and both macrophages and foam cells are integral components of the inflammatory cell phase. Conse-

quently, inflammatory cell volume fraction depends on oxLDL concentration. In addition, the concentration of f-cytokines is influenced by oxLDL, as oxLDL stimulates the production of f-cytokines. However, the toxic environment induced by oxLDL, beyond the threshold value  $c_1 = c_1^*$ , as explained in Eq. (16), leads to inflammatory cell death. Fig. 5a depicts the variation of inflammatory cell volume with oxLDL concentration when  $c_1^* = 1.05$  (oxLDL induced reference toxicity level) at various time  $t$ . Accordingly, we fix  $t = t_{\text{fix}}$  where  $t_{\text{fix}} = 10, 20, 25, 30$  etc. Corresponding to each  $t_{\text{fix}}$ , one can identify  $\varphi^f$  and  $c_1$  as the function of  $x(t = t_{\text{fix}})$  such that for each  $t = t_{\text{fix}}$  we get both the values of  $\varphi^f$  and  $c_1$  at each point of the plaque. The inflammatory cell population initially increases with  $c_1$  as they are produced when oxLDLs are metabolized. Beyond  $c_1 = c_1^*$ , the death of inflammatory cells begins due to the oxLDL-induced toxicity. Consequently, the amelioration of  $\varphi^f$  with respect to  $c_1$  ceases and tends to meet a nearly constant value (Fig. 5a).

As mentioned earlier, f-cytokines are secreted from inflammatory cells in the presence of oxLDL within the intima. Hence, the toxicity induced by oxLDL also impacts the concentration of f-cytokines. In Fig. 5b, the variation of f-cytokines with oxLDL at  $t_{\text{fix}} = 10, 20, 25, 30$  is shown. An initial surge of the f-cytokines can be seen in Fig. 5b with the concentration of oxLDL ( $c_1$ ), and the corresponding growth tends to flattened at the higher  $c_1$  due to the oxLDL-induced toxicity. Moreover, both  $c_1$  and  $c_2$  hike over time with a reduced decay rate within the plaque. It is essential to discuss the impact of f-cytokines on the volume of inflammatory cells within the intima. The concentration of f-cytokines influences the production of inflammatory cells by attracting excess monocytes or macrophages into the intima, where they further transform into foam cells. The corresponding feature is included in our modelling through the boundary condition (57). In Fig. 5c, we illustrate the change in inflammatory cell volume fraction against f-cytokines at different times  $t_{\text{fix}} = 10, 15, 20, 25$ . With the increasing f-cytokines, the volume fraction of inflammatory cells shows a monotonically increasing behaviour; however, it reaches a maximum value for a particular value of  $c_2$ . The corresponding maxima at different times considered are shown with a blue dot. It is observed that the locus of these maxima shows a monotonically increasing trend, which means at large times, the increasing volume fraction of inflammatory cells accelerates plaque growth. The dotted line represents the locus.

It seems that three factors, namely  $\varphi^f$ ,  $c_1$ , and  $c_2$ , collectively contribute to

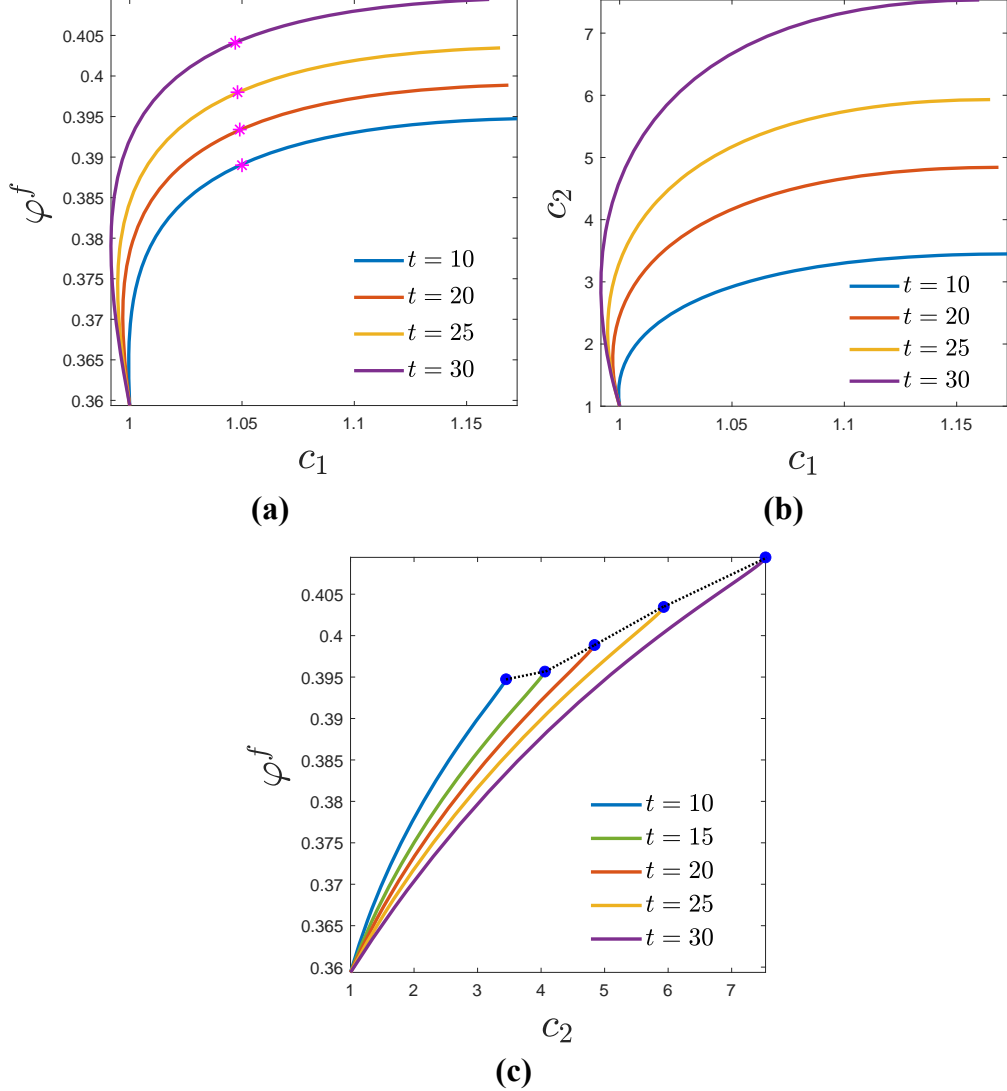


Figure 5: (a) Inflammatory cell volume variation with oxLDL concentration, (b) concentration of f-cytokines varies with oxLDL concentration, and (c) volume fraction of inflammatory cells concerning f-cytokine concentration at different time points. The star markers in (a) indicate the volume fraction of inflammatory cells corresponding to  $c_1^* = 1.05$ , and the blue dots in (c) represent the maximum volume of inflammatory cells at different times, with the dotted curve indicating its locus.

the growth of plaque depth. Fig. 6 displays the change in plaque width over

time (indicated by the solid blue line) and shows a rapid initial increase, followed by a gradual decrease in growth rate, which does not show any signs of plateauing. Hence, a question arises whether the growth rate of plaque width becomes flattened or not. However, it is clear that the speed with which the moving edge proceeds remains almost constant after an initial period. In order to answer this, we classify the behavior of the temporal variation of the plaque width as shown in Fig. 6 in three transitions. These are:  $0 \leq t \leq 3$ ;  $3 < t \leq 10$ ;  $t > 10$ . We then look for correlations in each zone as functions of  $\varrho_1$ ,  $\varrho_2$ ,  $\vartheta$  and  $t$ . Accordingly, we propose the following

$$l(t) = \begin{cases} 1 + \frac{1}{2^{\vartheta-2}} t^{\frac{1}{\vartheta+1}}, & 0 \leq t \leq 3, \\ 1 + \varrho_1 + \frac{1}{2^{\vartheta-1}} t^{\frac{1}{\vartheta}}, & 3 < t \leq 10, \\ 1 + \varrho_1 + \varrho_2 + \frac{1}{2^{\vartheta}} t^{\frac{1}{\vartheta-1}}, & t > 10. \end{cases} \quad (88)$$

The values of the parameters in the above-proposed function are set as follows:  $\vartheta = 3$ ,  $\varrho_1 \in [0.29, 0.3]$  and  $\varrho_2 \in [0.14, 0.15]$ , to ensure that the correlation becomes a reliable approximation of the plaque growth curve. Note that the number of transition zones in the growth curve is the same as the value of  $\vartheta$ . The dotted line in Fig. 6 represents the growth curve corresponding to the above-proposed correlation (88). The similarity in behavior between the two lines in Fig. 6 indicates that Eq. (88) is a reliable approximation of the solid line, which represents the plaque growth curve in this study. If we closely observe these temporal variation of the plaque growth (either the thick line or the dotted line), we can classify these zones in terms of risk that one may have. There is a rapid growth in the *zone 1* ( $0 \leq t \leq 3$ ) and hence this may be termed as '*early state of risk*'. Consequently, *zone 2* ( $3 < t \leq 10$ ) may be termed as '*advanced state of risk*' because by that time the plaque growth is high enough. Finally, *zone 3* ( $t > 10$ ) may be termed as the '*state of persistent risk*'. One may observe a parabolic nature of the plaque growth curve beyond  $t = 10$  which implies the risk of developing complications related to atherosclerosis in a patient. In this situation, atherosclerosis is expected to continue for a patient unless it is being treated. The correlations shown for the zone classification together with the nomenclature of the nature of risk are first of its kind in literature. Based on this classification, more importance may be given to the simulated results beyond  $t > 10$  days. Accordingly, we choose [10, 35] days as the range of time for our study. The parabolic nature indicates the inhibition of plaque growth due to the experience of normal stress from its surroundings within the intima.

The impact of oxLDL-induced toxicity on plaque growth is significant. Further details regarding this matter are discussed in the subsequent sections. According to this model, early atherosclerotic plaque expands towards the internal elastic lamina (IEL) and this behavior agrees with the reality. The growing plaque experiences a more considerable rigidity from IEL compared to the damaged endothelium. As a result, in later stages, the ever-increasing plaque has no way except to enter the lumen after causing further damage to the endothelium. This is why atherosclerosis narrows the lumen and prevents the blood flow.

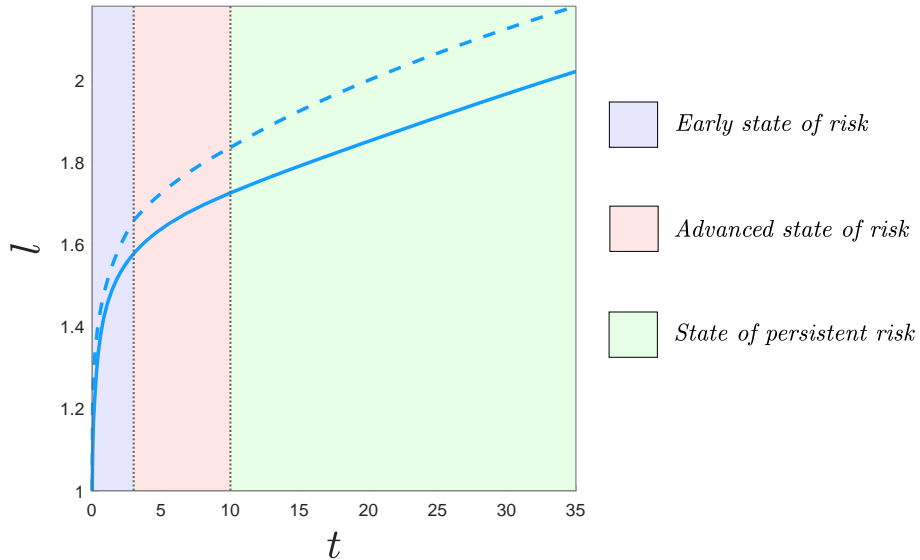


Figure 6: Evolution of plaque width  $l(t)$  over time  $t$ . The dashed curve represents the proposed function (88).

### 5.2.1. The Role of oxLDL and f-Cytokines Influxes $\nu_1$ , $\nu_2$ and $\nu_3$ on the Plaque Growth Behaviour

Influx parameters  $\nu_1$  (oxLDL),  $\nu_2$  (f-cytokines), and  $\nu_3$  (f-cytokines) on the model variables  $\varphi^f$ ,  $c_1$ , and  $c_2$ , it is imperative to express these model variables as functions of either spatial or temporal variables. This necessity arises because, at various instants of time, the variation of  $\varphi^f$  shows diverse behaviour at different locations within the intima depending upon the values of the parameters chosen for our discussion. Similar phenomena are expected

for  $c_1$  and  $c_2$ . Therefore, for the sake of convenience, it is decided to integrate  $\varphi^f$ ,  $c_1$ , and  $c_2$  within the range  $[0, l(t)]$  to obtain the following averaged variables respectively:

$$\text{Averaged Volume of Inflammatory Cells : } \langle \varphi^f \rangle = \frac{1}{l(t)} \int_{x=0}^{l(t)} \varphi^f(x, t) dx, \quad (89a)$$

$$\text{Averaged oxLDL Concentration : } \langle c_1 \rangle = \frac{1}{l(t)} \int_{x=0}^{l(t)} c_1(x, t) dx, \quad (89b)$$

and

$$\text{Averaged f-cytokines Concentration : } \langle c_2 \rangle = \frac{1}{l(t)} \int_{x=0}^{l(t)} c_2(x, t) dx. \quad (89c)$$

Henceforth, most of the discussion has been made based on above-averaged quantities. The integrals at the right-hand side of the above equations are evaluated using standard Newton's cotes formulae. The numerical solutions of  $\varphi^f$ ,  $c_1$ , and  $c_2$  are subjected to Simpson's 1/3 rule within the interval  $[0, l(t)]$  for each  $t \in [0, T]$ . Note that  $\langle \varphi^f \rangle$ ,  $\langle c_1 \rangle$ , and  $\langle c_2 \rangle$  are functions of time  $t$ . These quantities may exhibit unstable behaviour at the onset of the inflammatory process. Sometimes, even a small deviation in the parameter value can result in a significant variation in magnitude. Consequently, paying attention to the simulations some time steps later is imperative. Eventually, we choose a time interval of [10, 35] days to analyze further. Fig. 7a displays the temporal variation of average oxLDL concentration within time domain [10, 35] days corresponding to different influx rates  $\nu_1 = 0.01, 0.1, 0.2, 0.3$ . The parameter  $\nu_1$  represents a constant oxLDL influx rate into the intima through damaged endothelium. According to Chalmers et al. (2015),  $\nu_1$  can be considered proportional to the blood LDL level. Therefore, the higher magnitude of  $\nu_1$  suggests an increased concentration of LDL in blood. LDL molecules enter the intima through damaged endothelium, where free oxygen radicals oxidize them to become oxLDL. This oxidation process is speedy. The timescale for oxidation is infinitesimally small compared to plaque growth. Thus, it is more accurate to assume that oxLDL enters the intima from the lumen through the EII ( $x = 0$ ) rather than free lipids (LDL) influx. The concentration of oxLDL enhances throughout the intima with the influx parameter  $\nu_1$ . However, the average oxLDL concentration  $\langle c_1 \rangle$  reduces over time. With reducing  $\nu_1$ , a higher rate of decay of  $\langle c_1 \rangle$  is realized. The reduced influx rate of oxLDL corresponds to the situation when

the endothelium layer suffers minor damage. Similarly, a larger influx rate of oxLDL can be correlated with a major damaged endothelium. The influx parameter  $\nu_1$  plays a crucial role in elevating the concentration of f-cytokines within the intima, as depicted in Fig. 7b. The secretion of f-cytokines at the endothelium is influenced by ox-LDL, and higher  $\nu_1$  enhances the average oxLDL concentration within the intima (see Fig. 7a). Consequently, the concentration of f-cytokines is escalated with the higher magnitude of  $\nu_1$  due to increased concentration of free LDL within blood.

The level of f-cytokines controls the migration of macrophages into the intima. The flux of f-cytokines at the EII is directly proportional to the concentrations of oxLDL and f-cytokines, according to the boundary condition (57). Note that f-cytokines are primarily secreted from endothelial cells, and the corresponding flux is regulated by the parameters  $\nu_2$  and  $\nu_3$ . At the EII, the flux of f-cytokines is connected to the oxLDL concentration through the parameter  $\nu_2$ . At the same time,  $\nu_3$  regulates the flux of f-cytokines by controlling the corresponding concentration at the interface. Fig. 7c illustrates the variations in the average f-cytokine concentration over time corresponding to  $\nu_2 = 0.01, 0.04, 0.07, 0.1$  when  $\nu_1 = 0.2$  and  $\nu_3 = 0.001$ . Larger values of  $\nu_2$  result in a higher influx of f-cytokines at the EII. Consequently, it becomes responsible for enhancing the average f-cytokine concentration within the intima, as shown in Fig. 7c. Similarly, the more significant value of the influx parameter  $\nu_3$  escalates the influx of f-cytokines at the EII. As a result, the average concentration of f-cytokines ( $\langle c_2 \rangle$ ) within the intima rises with higher  $\nu_3$ , as evidenced in Fig. 7d.

It is worth noting that inflammatory cells primarily contribute to early plaque development. Therefore, we must emphasize the roles of influx parameters  $\nu_1$ ,  $\nu_2$ , and  $\nu_3$  on the average volume of inflammatory cells  $\langle \varphi^f \rangle$ . In this regard, Fig. 8a-8c depict the individual impact of  $\nu_1$ ,  $\nu_2$ , and  $\nu_3$  on  $\langle \varphi^f \rangle$  respectively. In all these three cases, the average volume of inflammatory cells grows with  $t$  within the interval [10, 35].  $\nu_1$ , which corresponds to the influx of oxLDL, becomes responsible for inflammatory cell production. Higher  $\nu_1$  correlates with increased concentrations of oxLDL, triggering an inflammatory response through pro-inflammatory f-cytokines. This process draws monocytes (macrophages within the intima) from the bloodstream to the intima, where they further transform into foam cells by consuming oxLDL. Consequently, one can anticipate a higher production of inflammatory cells.

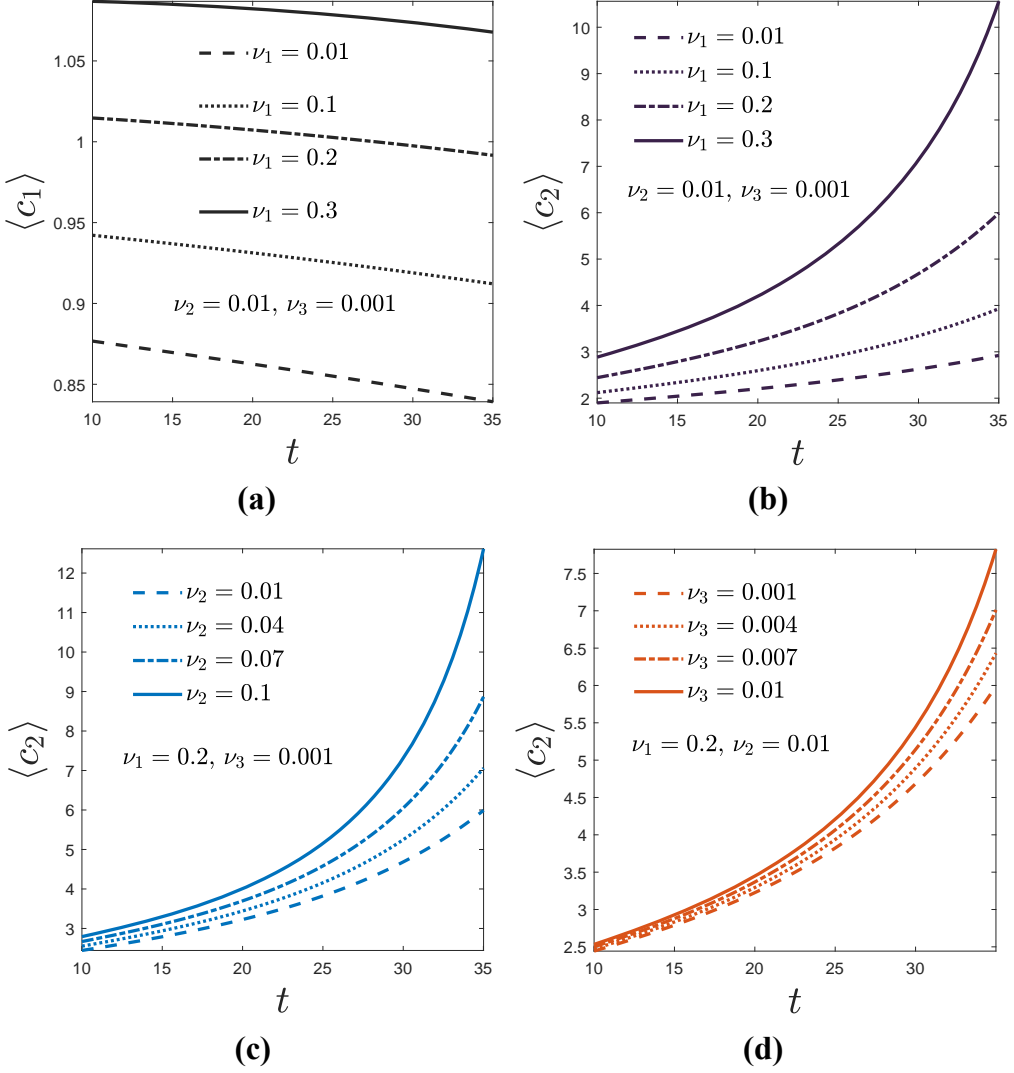


Figure 7: (a) Average oxLDL concentration for various  $\nu_1$  when  $\nu_2 = 0.01$  and  $\nu_3 = 0.001$ . The average concentration of f-cytokines versus  $t$  for various: (b)  $\nu_1$  (when  $\nu_2 = 0.01$  and  $\nu_3 = 0.001$ ), (c)  $\nu_2$  (when  $\nu_1 = 0.2$  and  $\nu_3 = 0.001$ ), and (d)  $\nu_3$  (when  $\nu_1 = 0.2$  and  $\nu_2 = 0.01$ ).

Fig. 8a supports this phenomenon. The other two influx parameters,  $\nu_2$  and  $\nu_3$ , are found to exhibit a positive response on the growth of inflammatory cell volume ( $\langle \varphi^f \rangle$ ) throughout the intima as evidenced in Fig. 8b and 8c,

respectively. Fig. 8b illustrates the variation of  $\nu_2$  in the averaged inflammatory cell volume fraction, while Fig. 8c displays the variation of  $\nu_3$ . It can be observed that both  $\nu_2$  and  $\nu_3$  contribute to the inflammatory cell volume fraction ( $\langle \varphi^f \rangle$ ) with their respective elevations. The positive role of these influx parameters in influencing the average f-cytokines concentration within the intima has already been investigated. Consequently, the recruitment of macrophages from the bloodstream and, subsequently, the production of new inflammatory cells increase.

As noted earlier, early plaque development primarily depends on the inflammatory cell phase in the presence of oxLDL molecules within the intima and active f-cytokines gradient. Consequently, the plaque width is controlled by each of  $\nu_1$ ,  $\nu_2$ , and  $\nu_3$  depicted in Fig. ref{Figure8a}-ref{Figure8c}, respectively. We have already classified plaque growth and its impact on early atherosclerosis into three regimes: early state, advanced state, and persistent state of risk. These three parameters mainly affect the third regime. Hence, one can comprehend the long-term impact of these parameters. Fig. 9a illustrates an exciting feature. Plaque growth was found to be reduced at a fixed time with larger values of  $\nu_1$ . This reduction was observed to be more pronounced after a long time, indicating a potential long-term effect of  $\nu_1$  on plaque growth. Higher  $\nu_1$  ( $> 0.1$ ) leads to a significant increase in oxLDL concentration within the intima, inevitably resulting in a substantial buildup of foam cells within this layer. However, beyond a specific threshold concentration of oxLDL, it becomes toxic to inflammatory cells, initiating their death due to oxLDL-induced toxicity. Consequently, the width of the plaque, formed through the deposition of inflammatory cells, decreases at larger  $\nu_1$ , indicating a reduction in the plaque growth rate. Additionally, the free oxLDLs released from the dead foam cells cause further recruitment of new inflammatory cells. Consequently, the overall inflammatory process persists, leading to the non-flattened growth rate of plaque. On the other hand, with a low influx rate of oxLDL, the impact of induced toxicity becomes marginal over the inflammatory cell population. When the oxLDL influx rate  $\nu_1 \leq 0.1$ , a marginal change in the plaque depth occurs for a further smaller magnitude of  $\nu_1$ . In this situation, the foam cells deposited within the intima (though not in large numbers) do not significantly encounter the toxic effect. As a result, plaque depth sharply increases over time due to its resistance to oxLDL-induced toxicity. Now, the regime of persistent risk has become more expansive. It is important to note that the growth rate

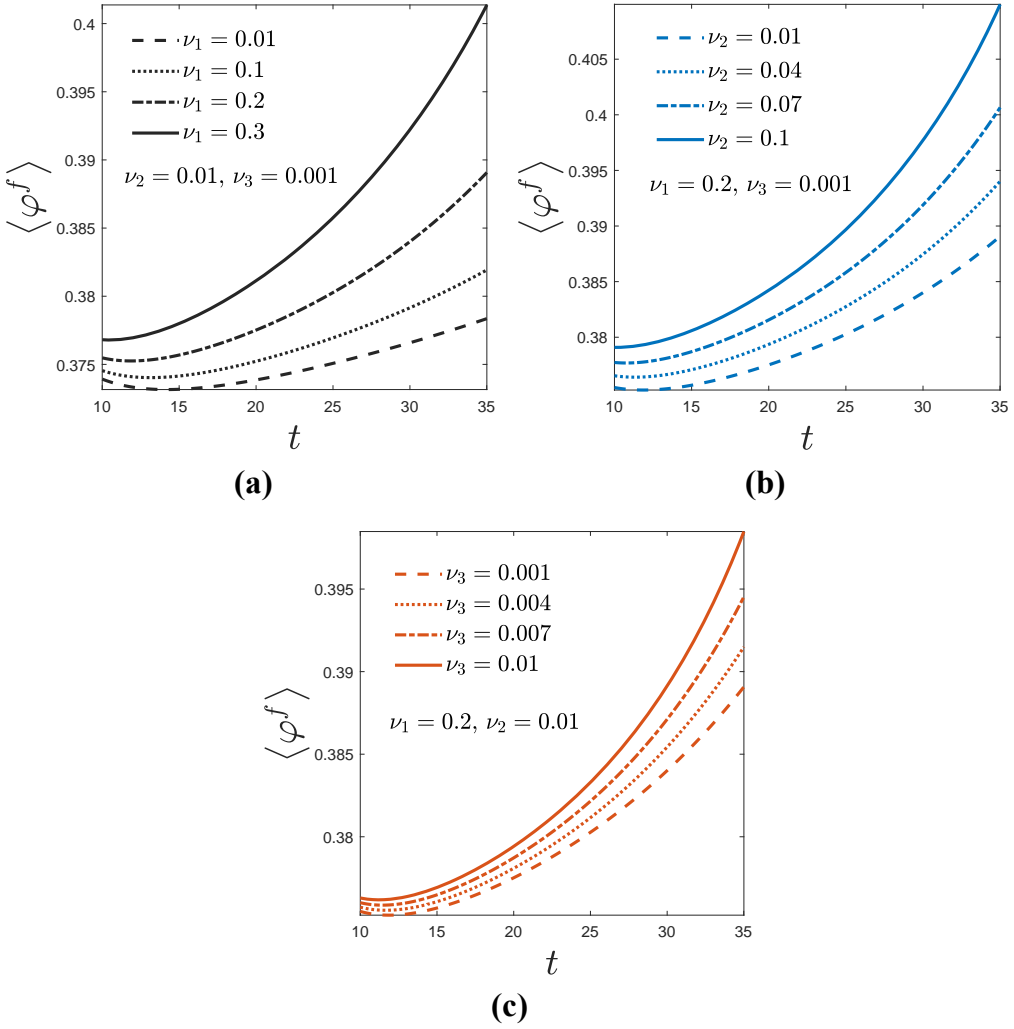


Figure 8: Variation of inflammatory cell average volume fraction for different (a)  $\nu_1$ , (b)  $\nu_2$ , and (c)  $\nu_3$ .

of plaque tends to slow down unless sufficient dead materials are produced from the inflammatory cells. However, this aspect is outside the scope of the current study. As a result, the advancement of plaque growth gets delayed in advanced stages. The present study shows that oxLDL-induced toxicity is a critical factor in the plaque growth stabilization.

The roles of influx parameters  $\nu_2$  and  $\nu_3$  corresponding to f-cytokines over

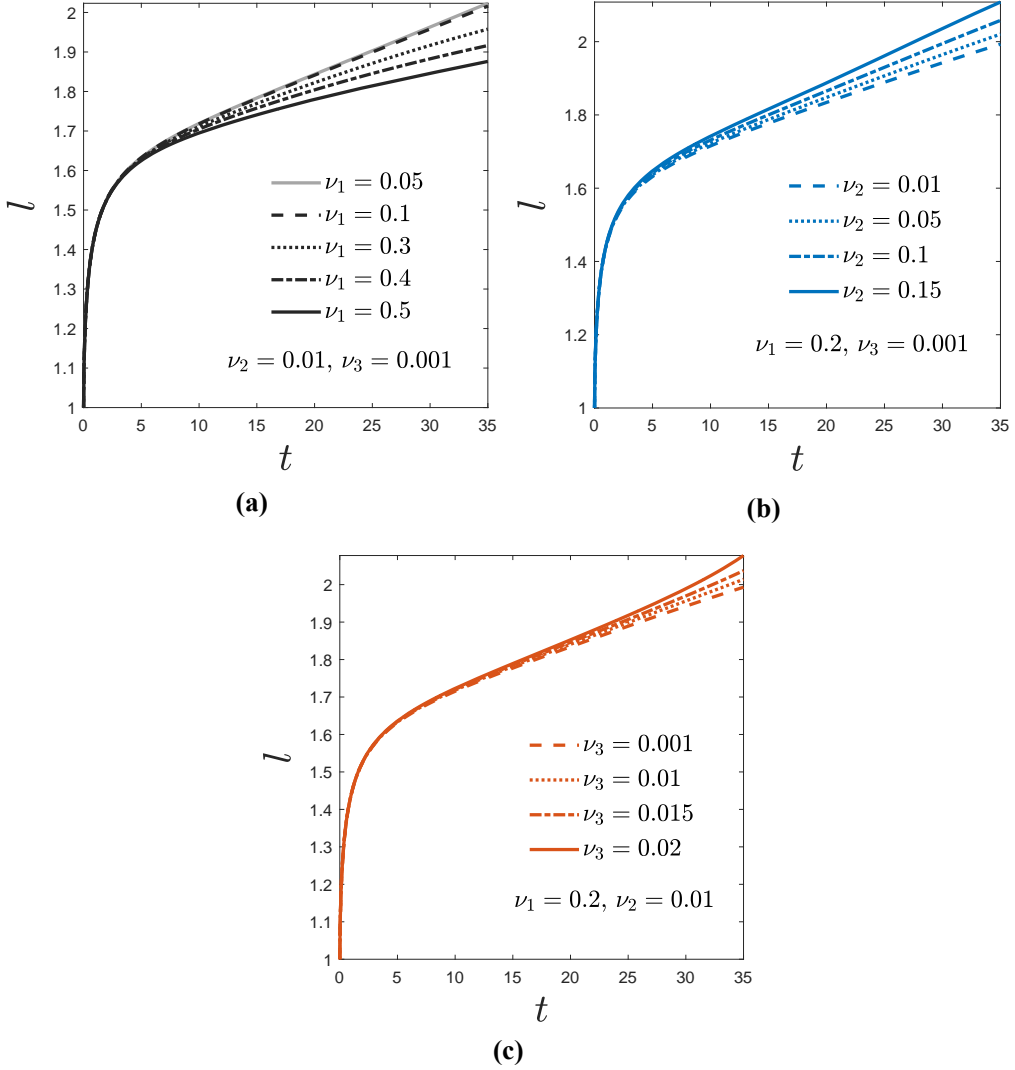


Figure 9: Plaque width for various (a)  $\nu_1$ , (b)  $\nu_2$ , and (c)  $\nu_3$ .

the plaque growth are found to behave opposite to  $\nu_1$  (see Fig. 9b and 9c). A notable impact of f-cytokines within intima is experienced at the immense values of  $\nu_2$  and  $\nu_3$  that consequences a high concentration of f-cytokines. Consequently, the inflammatory response causes more macrophages to migrate to the intima under the influence of increased f-cytokines, resulting in an increased macrophage population and, thus, foam cells. Hence, further

recruitment and proliferation of inflammatory cells occur within the intima. This incident leads to an elevated growth rate in plaque width. Consequently, the growth in early plaque width is positively correlated with the values of  $\nu_2$  (Fig. 9b) and  $\nu_3$  (Fig. 9c). The comprehensive analysis affirms that the oxLDL influx parameter  $\nu_1$  positively influences the non-flattened plaque growth profile with respect to time, primarily attributed to oxLDL-induced toxicity. On the other hand, the influx parameters  $\nu_2$  and  $\nu_3$  associated with f-cytokines disrupt the flattened behaviour.

#### 5.2.2. *Effect of Varied Toxicity Level Induced by oxLDL ( $c_1^*$ )*

As discussed earlier, the toxicity caused by oxLDL leads to inflammatory cell death, which contributes significantly to plaque formation. The impact of different toxicity levels, denoted by  $c_1^*$ , on the growth of inflammatory cell volume and plaque width is shown in Figs. 10a-10b respectively. Inflammatory cells suffer death when oxLDL reaches its toxicity level. Higher levels of toxicity result in increased growth of inflammatory cells due to their rapid proliferation and absence of cell death at that level of toxicity. This incident leads to an increased volume fraction of inflammatory cells as  $c_1^*$  rises (Fig. 10a). Moreover, as depicted in Fig. 10b, a rise in  $c_1^*$  corresponds to an increased plaque width. As the concentration of  $c_1^*$  increases, the population of inflammatory cells also grows, causing the plaque to form faster due to the deposition of these cells.

#### 5.3. *Qualitative Agreement with the Clinical Studies*

We attempt to compare specific results from this study with the existing clinical studies done by Meyer et al. (1996) and Stangeby and Ethier (2002). Accordingly, the LDL concentrations within the arterial intima are picked up from these studies corresponding to transmural pressures of  $p = 70, 120, 160$  mmHg. The LDL concentration data are extracted using the 'Grabit' toolbox of MATLAB R2021a. They are normalized first before comparing with the oxLDL concentrations obtained from the present study at each point within the intima. The normalization process is done so that the domain of clinical data maps onto that of the present study through a suitable transformation. Such transformation pivots more on the qualitative agreement rather than the quantitative. Note that the present study is focused on oxLDL rather than LDL, as oxidization takes place in a short time while growth is a long-scale process. Figs. 11a and 11b delineate the above-mentioned comparative study. In the first plot, the concentrations of oxLDL (this study) and LDL

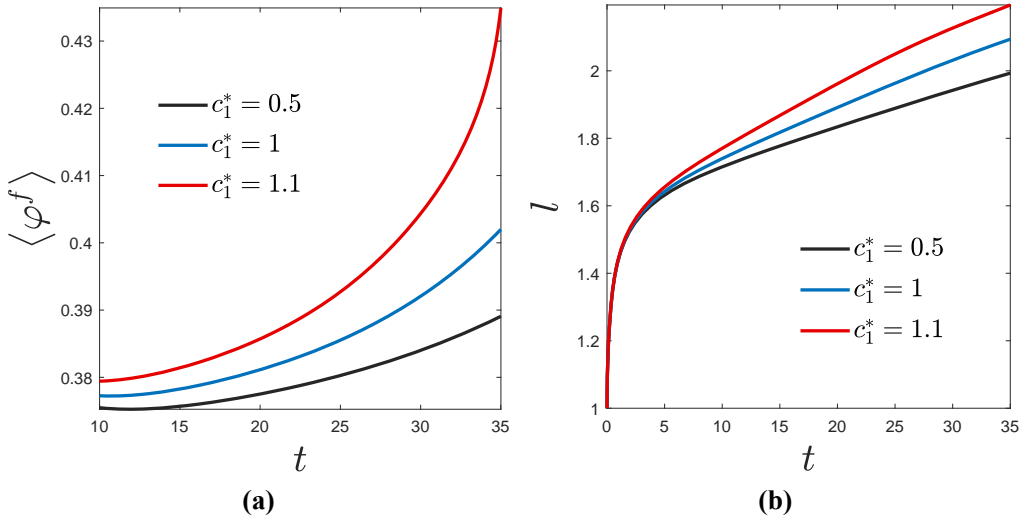


Figure 10: (a) Distributions of inflammatory cell average volume fraction, and (b) plaque width variation with  $t$  within the intima corresponding to various  $c_1^*$ .

(Stangeby and Ethier (2002)) are shown for  $\nu_1 = 0.2, 0.3$  and  $p = 120, 160$ , respectively. The following figure compares the present study and Meyer et al. (1996), corresponding to  $\nu_1 = 0.1, 0.2, 0.3$  and  $p = 70, 120, 160$  respectively. A good qualitative agreement between the clinical and present studies has been observed, and the comparisons show that the normalized LDL (obtained from Meyer et al. (1996) and Stangeby and Ethier (2002)) and oxLDL (obtained from the current study) concentrations behave similarly. Both are highly concentrated near the lumen or EII and decrease toward the media or arterial wall.

## 6. Summary and Conclusions

Multiphase mixture theory models are adopted to investigate the role of macrophages and foam cells in the early stages of atherosclerosis. This study found that oxLDL-induced toxicity plays a significant role in the early growth of plaque. Macrophages consume oxLDL to become foam cells, but overconsumption causes toxicity, which can lead to the death of foam cells. The study systematically analyzed the activity of oxLDL, the role of f-cytokines, and the behaviour of inflammatory cells, such as foam cells and macrophages. Plaque growth is limited to the intima and is subjected to constant inward

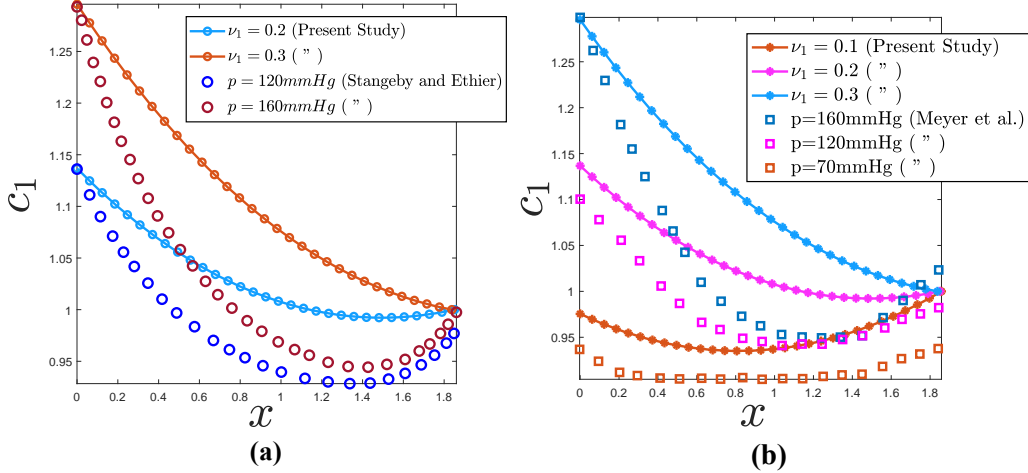


Figure 11: Comparison between the present study and the clinical studies done by (a) Stangeby and Ethier (2002) and (b) Meyer et al. (1996) along the variation of oxLDL concentration with distance from the intima-endothelium interface corresponding to various  $\nu_1$  for different pressures.

normal stress from the surrounding intima materials and internal elastic lamina. The study identified three regions corresponding to early plaque growth: early state, advanced state and persistent state of risk. The growth is initially steep but gradually flattened into a parabolic profile due to the oxLDL-induced toxicity effect. Furthermore, the toxic effect of oxLDL impacts the functioning of inflammatory cells and f-cytokines. Correspondingly, a correlation (88) is proposed that dictates the plaque growth process when the oxLDL-induced toxicity issue is taken into consideration.

This study introduces three parameters  $\nu_1$ ,  $\nu_2$ , and  $\nu_3$  that determine the influxes of substances in the plaque. The first parameter,  $\nu_1$ , is associated with the influx of oxLDL, while the second and third parameters,  $\nu_2$  and  $\nu_3$ , correspond to the influx of f-cytokines. A higher influx of oxLDL leads to a better-flattened growth rate of plaque width. However, a flattened plaque growth rate increases the risk of oxLDL-induced toxicity. The influx parameters  $\nu_2$  and  $\nu_3$  behave in an opposite manner to the oxLDL influx parameter during plaque development. Both these parameters are responsible for the growth of the inflammatory cell phase and, thus, plaque width. The present analysis indicates that the oxLDL influx parameter positively influences the flattening of the plaque growth rate. On the other hand, the influx

parameters associated with f-cytokines destabilize the flattening. Additionally, f-cytokines can reduce the overall inflammatory process by decreasing the recruitment of inflammatory cells from the bloodstream to the intima layer through the damaged endothelium. Moreover, we observed a significant change in the plaque growth profile due to the variation in the toxicity level,  $c_1^*$ . A higher toxicity level primarily indicates a reduction in the death of inflammatory cells up to that level and the proliferation of more inflammatory cells, thereby accelerating plaque growth.

The present study simplifies several complex mechanisms involved in early atherosclerosis to understand plaque formation. It is illustrated that plaque formation relies on oxLDL ingestion and macrophage chemotaxis. The role of oxLDL toxicity in plaque growth is established. This study would help develop new therapeutic strategies to prevent the progression of atherosclerosis in its early stages. Moreover, the impact of High-density lipoprotein (HDL) on plaque development may be even more significant in the presence of oxLDL-induced toxicity.

### Acknowledgements

First author A. S. Pramanik acknowledges University Grants Commission (UGC), Govt. of India for providing Senior Research Fellowship (NET-JRF, Award Letter Number: 1149/(CSIR-UGC NET DEC-2018)). Second author B. Dey acknowledges University Research Assistance (Ref. 1516/R-2020 dated 01.06.2020) of University of North Bengal for supporting this work.

### *Appendix A: Leading order coefficients*

$$(\varphi^n)^{(0)} = 1 - (\varphi^f)^{(0)},$$

$$\nabla^f{}^{(0)} = (\varphi^f)^{(0)}(\varphi^n)^{(0)} \frac{s_0 c_2^{(0)}}{1 + s_1 c_2^{(0)}} + (\varphi^f)^{(0)}(\varphi^n)^{(0)} \frac{s_2 c_1^{(0)}}{1 + s_3 c_1^{(0)}} - (\varphi^f)^{(0)} \frac{s_4 + s_5 c_1^{(0)}}{1 + s_6 c_1^{(0)}} \mathcal{H}(c_1^{(0)} - c_1^*),$$

$$Q_1^{(0)} = (\varphi^f)^{(0)}(\varphi^n)^{(0)} q_0 c_1^{(0)} - (\varphi^f)^{(0)}(\varphi^n)^{(0)} q_2 c_1^{(0)},$$

$$Q_2^{(0)} = (\varphi^n)^{(0)} q_3 c_2^{(0)} - (\varphi^n)^{(0)} (\varphi^f)^{(0)} q_4 c_1^{(0)} c_2^{(0)},$$

$$\Sigma^{(0)} = \frac{\left( (\varphi^f)^{(0)} - \varphi^* \right)}{\left( 1 - (\varphi^f)^{(0)} \right)^2} \mathcal{H}((\varphi^f)^{(0)} - \varphi^*),$$

$$\Lambda^{(0)} = \frac{\chi}{1 + \left( \kappa c_2^{(0)} \right)^m}.$$

### Appendix B: $\mathcal{O}(q_1)$ coefficients

$$(\varphi^n)^{(1)} = -(\varphi^f)^{(1)},$$

$$\begin{aligned} \nabla^{(1)} &= \left( (\varphi^f)^{(0)} (\varphi^n)^{(1)} + (\varphi^f)^{(1)} (\varphi^n)^{(0)} \right) \frac{s_0 c_2^{(0)}}{1 + s_1 c_2^{(0)}} + (\varphi^f)^{(0)} (\varphi^n)^{(0)} \left( \frac{s_0 c_2^{(1)}}{1 + s_1 c_2^{(0)}} - \frac{s_0 s_1 c_2^{(0)} c_2^{(1)}}{\left( 1 + s_1 c_2^{(0)} \right)^2} \right) \\ &\quad + \left( (\varphi^f)^{(0)} (\varphi^n)^{(1)} + (\varphi^f)^{(1)} \varphi^{n(0)} \right) \frac{s_2 c_1^{(0)}}{1 + s_3 c_1^{(0)}} + (\varphi^f)^{(0)} (\varphi^n)^{(0)} \left( \frac{s_2 c_1^{(1)}}{1 + s_3 c_1^{(0)}} - \frac{s_2 s_3 c_1^{(0)} c_1^{(1)}}{\left( 1 + s_3 c_1^{(0)} \right)^2} \right) \\ &\quad - \left( (\varphi^f)^{(1)} \frac{s_4 + s_5 c_1^{(0)}}{1 + s_6 c_1^{(0)}} + (\varphi^f)^{(0)} \left( \frac{s_5 c_1^{(1)}}{1 + s_6 c_1^{(0)}} - \frac{s_6 c_1^{(1)} (s_4 + s_5 c_1^{(0)})}{\left( 1 + s_6 c_1^{(0)} \right)^2} \right) \right) \mathcal{H}(c_1^{(1)} - c_1^*), \end{aligned}$$

$$\begin{aligned} Q_1^{(1)} &= (\varphi^f)^{(0)} (\varphi^n)^{(0)} q_0 \left( c_1^{(1)} - (c_1^{(0)})^2 \right) + \left( (\varphi^f)^{(0)} (\varphi^n)^{(1)} + (\varphi^f)^{(1)} (\varphi^n)^{(0)} \right) q_0 c_1^{(0)} \\ &\quad - (\varphi^f)^{(0)} (\varphi^n)^{(0)} q_2 c_1^{(1)} - \left( (\varphi^f)^{(0)} (\varphi^n)^{(1)} + (\varphi^f)^{(1)} (\varphi^n)^{(0)} \right) q_2 c_1^{(0)}, \end{aligned}$$

$$\begin{aligned} Q_2^{(1)} &= q_3 \left( (\varphi^n)^{(0)} c_2^{(1)} + (\varphi^n)^{(1)} c_2^{(0)} \right) - q_4 \left( (\varphi^n)^{(0)} (\varphi^f)^{(1)} + (\varphi^n)^{(1)} (\varphi^f)^{(0)} \right) c_1^{(0)} c_2^{(0)} \\ &\quad - q_4 (\varphi^n)^{(0)} (\varphi^f)^{(0)} \left( c_1^{(0)} c_2^{(1)} + c_1^{(1)} c_2^{(0)} \right), \end{aligned}$$

$$\Sigma^{(1)} = \left( \frac{(\varphi^f)^{(1)}}{\left(1 - (\varphi^f)^{(0)}\right)^2} + \frac{2((\varphi^f)^{(0)} - \varphi^*)(\varphi^f)^{(1)}}{\left(1 - (\varphi^f)^{(0)}\right)^3} \right) \mathcal{H}((\varphi^f)^{(1)} - \varphi^*),$$

$$\Lambda^{(1)} = -\frac{m\chi\kappa^m \left(c_2^{(0)}\right)^{m-1} c_2^{(1)}}{\left(1 + \kappa^m \left(c_2^{(0)}\right)^m\right)^2}.$$

## References

Ahmed, I.U., Byrne, H.M., Myerscough, M.R., 2023. Macrophage anti-inflammatory behaviour in a multiphase model of atherosclerotic plaque development. *Bulletin of Mathematical Biology* 85, 37.

Alam, M., Dey, B., Raja Sekhar, G.P., 2019. Mathematical modeling and analysis of hydroelastodynamics inside a solid tumor containing deformable tissue. *ZAMM-Journal of Applied Mathematics and Mechanics/Zeitschrift für Angewandte Mathematik und Mechanik* 99, e201800223.

Badimon, L., et al., 1990. Regression of atherosclerotic lesions by high density lipoprotein plasma fraction in the cholesterol-fed rabbit. *The Journal of clinical investigation* 85, 1234–1241.

Berliner, J.A., Navab, M., Fogelman, A.M., Frank, J.S., Demer, L.L., Edwards, P.A., Watson, A.D., Lusis, A.J., 1995. Atherosclerosis: basic mechanisms: oxidation, inflammation, and genetics. *Circulation* 91, 2488–2496.

Bonithon-Kopp, C., Touboul, P.J., Berr, C., Leroux, C., Mainard, F., Courbon, D., Ducimetiere, P., 1996. Relation of intima-media thickness to atherosclerotic plaques in carotid arteries: the vascular aging (eva) study. *Arteriosclerosis, Thrombosis, and Vascular biology* 16, 310–316.

van den Bos, E., Walbaum, S., Horsthemke, M., Bachg, A.C., Hanley, P.J., 2020. Time-lapse imaging of mouse macrophage chemotaxis. *Journal of Visualized Experiments* , e60750.

Breward, C., Byrne, H., Lewis, C., 2002. The role of cell-cell interactions in a two-phase model for avascular tumour growth. *Journal of Mathematical Biology* 45, 125–152.

Breward, C.J., Byrne, H.M., Lewis, C.E., 2003. A multiphase model describing vascular tumour growth. *Bulletin of Mathematical Biology* 65, 609–640.

Byrne, H., Preziosi, L., 2003. Modelling solid tumour growth using the theory of mixtures. *Mathematical medicine and biology: a journal of the IMA* 20, 341–366.

Byrne, H.M., King, J.R., McElwain, D.S., Preziosi, L., 2003. A two-phase model of solid tumour growth. *Applied Mathematics Letters* 16, 567–573.

Calvez, V., Ebde, A., Meunier, N., Raoult, A., 2009. Mathematical modelling of the atherosclerotic plaque formation, in: *Esaim: Proceedings*, EDP Sciences. pp. 1–12.

Calvez, V., Houot, J.G., Meunier, N., Raoult, A., Rusnakova, G., 2010. Mathematical and numerical modeling of early atherosclerotic lesions, in: *ESAIM: Proceedings*, EDP Sciences. pp. 1–14.

Chalmers, A.D., Bursill, C.A., Myerscough, M.R., 2017. Nonlinear dynamics of early atherosclerotic plaque formation may determine the efficacy of high density lipoproteins (hdl) in plaque regression. *PLoS One* 12, e0187674.

Chalmers, A.D., Cohen, A., Bursill, C.A., Myerscough, M.R., 2015. Bifurcation and dynamics in a mathematical model of early atherosclerosis. *Journal of Mathematical Biology* 71, 1451–1480.

Channon, K.M., 2006. The endothelium and the pathogenesis of atherosclerosis. *Medicine* 34, 173–177.

Chatzizisis, Y.S., Coskun, A.U., Jonas, M., Edelman, E.R., Feldman, C.L., Stone, P.H., 2007. Role of endothelial shear stress in the natural history of coronary atherosclerosis and vascular remodeling: molecular, cellular, and vascular behavior. *Journal of the American College of Cardiology* 49, 2379–2393.

Chen, D., Roda, J.M., Marsh, C.B., Eubank, T.D., Friedman, A., 2012. Hypoxia inducible factors-mediated inhibition of cancer by gm-csf: a mathematical model. *Bulletin of Mathematical Biology* 74, 2752–2777.

Cobbold, C., Sherratt, J., Maxwell, S., 2002. Lipoprotein oxidation and its significance for atherosclerosis: a mathematical approach. *Bulletin of Mathematical Biology* 64, 65–95.

Cohen, A., Myerscough, M.R., Thompson, R.S., 2014. Athero-protective effects of high density lipoproteins (hdl): an ode model of the early stages of atherosclerosis. *Bulletin of Mathematical Biology* 76, 1117–1142.

Davies, M., Woolf, N., 1993. Atherosclerosis: what is it and why does it occur? *British Heart Journal* 69, S3.

Dey, B., Raja Sekhar, G.P., 2016. Hydrodynamics and convection enhanced macromolecular fluid transport in soft biological tissues: Application to solid tumor. *Journal of Theoretical Biology* 395, 62–86.

Dey, B., Raja Sekhar, G.P., Mukhopadhyay, S.K., 2018. In vivo mimicking model for solid tumor towards hydromechanics of tissue deformation and creation of necrosis. *Journal of biological physics* 44, 361–400.

El Khatib, N., Génieys, S., Kazmierczak, B., Volpert, V., 2009. Mathematical modelling of atherosclerosis as an inflammatory disease. *Philosophical Transactions of the Royal Society A: Mathematical, Physical and Engineering Sciences* 367, 4877–4886.

El Khatib, N., Génieys, S., Kazmierczak, B., Volpert, V., 2012. Reaction–diffusion model of atherosclerosis development. *Journal of Mathematical Biology* 65, 349–374.

El Khatib, N., Génieys, S., Volpert, V., 2007. Atherosclerosis initiation modeled as an inflammatory process. *Mathematical Modelling of Natural Phenomena* 2, 126–141.

Feng, B., Yao, P.M., Li, Y., Devlin, C.M., Zhang, D., Harding, H.P., Sweeney, M., Rong, J.X., Kuriakose, G., Fisher, E.A., et al., 2003. The endoplasmic reticulum is the site of cholesterol-induced cytotoxicity in macrophages. *Nature cell biology* 5, 781–792.

Filipovic, N., Teng, Z., Radovic, M., Saveljic, I., Fotiadis, D., Parodi, O., 2013. Computer simulation of three-dimensional plaque formation and progression in the carotid artery. *Medical & Biological Engineering & computing* 51, 607–616.

Furchtgott, R.F., 1999. Endothelium-derived relaxing factor: discovery, early studies, and identification as nitric oxide. *Bioscience Reports* 19, 235–251.

Gotoh, N., Graham, A., Nikl, E., Darley-Usmar, V., 1993. Inhibition of glutathione synthesis increases the toxicity of oxidized low-density lipoprotein to human monocytes and macrophages. *Biochemical Journal* 296, 151–154.

Grootaert, M.O., da Costa Martins, P.A., Bitsch, N., Pintelon, I., De Meyer, G.R., Martinet, W., Schrijvers, D.M., 2015. Defective autophagy in vascular smooth muscle cells accelerates senescence and promotes neointima formation and atherogenesis. *Autophagy* 11, 2014–2032.

Gui, T., Shimokado, A., Sun, Y., Akasaka, T., Muragaki, Y., 2012. Diverse roles of macrophages in atherosclerosis: from inflammatory biology to biomarker discovery. *Mediators of Inflammation* 2012.

Han, K., Hong, K., Park, J., Ko, J., Kang, D., Park, S., 2004. Crp promotes mcp-1 mediated chemotaxis through upregulating ccr2 expression in human monocytes. *Circulation* 109, 2566–2571.

Hansson, G.K., Libby, P., 2006. The immune response in atherosclerosis: a double-edged sword. *Nature Reviews Immunology* 6, 508–519.

Hansson, G.K., Robertson, A.K.L., Söderberg-Nauclér, C., 2006. Inflammation and atherosclerosis. *Annual Review of Pathology: Mechanisms of Disease* 1, 297–329.

Hao, W., Friedman, A., 2014. The ldl-hdl profile determines the risk of atherosclerosis: a mathematical model. *PLoS One* 9, e90497.

Hegyi, L., Skepper, J.N., CARY, N.R., MITCHINSON, M.J., 1996. Foam cell apoptosis and the development of the lipid core of human atherosclerosis. *The Journal of Pathology* 180, 423–429.

Hillen, T., Painter, K.J., 2009. A user's guide to pde models for chemotaxis. *Journal of Mathematical Biology* 58, 183–217.

Hoffmann, K.A., Chiang, S.T., 2000. Computational fluid dynamics volume i. Engineering Education System .

Hubbard, M., Byrne, H., 2013. Multiphase modelling of vascular tumour growth in two spatial dimensions. *Journal of theoretical biology* 316, 70–89.

Ibragimov, A., McNeal, C., Ritter, L., Walton, J., 2005. A mathematical model of atherogenesis as an inflammatory response. *Mathematical Medicine and Biology* 22, 305–333.

Kim, Y., Friedman, A., 2010. Interaction of tumor with its microenvironment: A mathematical model. *Bulletin of Mathematical Biology* 72, 1029–1068.

Korshunov, V.A., Schwartz, S.M., Berk, B.C., 2007. Vascular remodeling: hemodynamic and biochemical mechanisms underlying glagov's phenomenon. *Arteriosclerosis, Thrombosis, and Vascular Biology* 27, 1722–1728.

Kumar, P., Dey, B., Raja Sekhar, G.P., 2018. Nutrient transport through deformable cylindrical scaffold inside a bioreactor: an application to tissue engineering. *International Journal of Engineering Science* 127, 201–216.

Lee, T., Baines, M.J., Langdon, S., Tindall, M.J., 2013. A moving mesh approach for modelling avascular tumour growth. *Applied Numerical Mathematics* 72, 99–114.

Libby, P., Ridker, P.M., Maseri, A., 2002. Inflammation and atherosclerosis. *Circulation* 105, 1135–1143.

Liu, L.K., Lee, H.J., Shih, Y.W., Chyau, C.C., Wang, C.J., 2008. Mulberry anthocyanin extracts inhibit ldl oxidation and macrophage-derived foam cell formation induced by oxidative ldl. *Journal of Food Science* 73, H113–H121.

Lusis, A., 2000. Atherosclerosis. *Nature* 407, 233–241.

Marchant, C.E., Van Der Wen, C., Law, N.S., Hardwick, S.J., Carpenter, K.L., Hutchinson, M.J., 1996. Oxidation of low-density lipoprotein by human monocyte-macrophages results in toxicity to the oxidising culture. *Free Radical Research* 24, 333–342.

McKay, C., McKee, S., Mottram, N., Mulholland, T., Wilson, S., Kennedy, S., Wadsworth, R., 2005. Towards a model of atherosclerosis. University of Strathclyde , 1–29.

Meyer, G., Merval, R.g., Tedgui, A., 1996. Effects of pressure-induced stretch and convection on low-density lipoprotein and albumin uptake in the rabbit aortic wall. *Circulation Research* 79, 532–540.

Newby, A.C., Zaltsman, A.B., 1999. Fibrous cap formation or destruction—the critical importance of vascular smooth muscle cell proliferation, migration and matrix formation. *Cardiovascular Research* 41, 345–360.

Ougrinovskaia, A., Thompson, R.S., Myerscough, M.R., 2010. An ode model of early stages of atherosclerosis: mechanisms of the inflammatory response. *Bulletin of Mathematical Biology* 72, 1534–1561.

Prakash, J., Raja Sekhar, G.P., De, S., Böhm, M., 2010. A criterion to avoid starvation zones for convection–diffusion–reaction problem inside a porous biological pellet under oscillatory flow. *International Journal of Engineering Science* 48, 693–707.

Pramanik, A.S., Dey, B., Karmakar, T., Saha, K., 2023. Two-phase modeling of fluid injection inside subcutaneous layer of skin. *International Journal of Engineering Science* 192, 103935.

Ross, R., 1999. Atherosclerosis—an inflammatory disease. *New England Journal of Medicine* 340, 115–126.

Saulnier-Blache, J.S., Wilson, R., Klavins, K., Graham, D., Alesutan, I., Kastenmüller, G., Wang-Sattler, R., Adamski, J., Roden, M., Rathmann, W., et al., 2018. Ldlr-/- and apoe-/- mice better mimic the human metabolite signature of increased carotid intima media thickness compared to other animal models of cardiovascular disease. *Atherosclerosis* 276, 140–147.

Stangeby, D.K., Ethier, C.R., 2002. Coupled computational analysis of arterial ldl transport—effects of hypertension. *Computer Methods in Biomechanics & Biomedical Engineering* 5, 233–241.

Tabas, I., et al., 2002. Consequences of cellular cholesterol accumulation: basic concepts and physiological implications. *The Journal of clinical investigation* 110, 905–911.

Tangirala, R.K., Tsukamoto, K., Chun, S.H., Usher, D., Pure, E., Rader, D.J., 1999. Regression of atherosclerosis induced by liver-directed gene transfer of apolipoprotein ai in mice. *Circulation* 100, 1816–1822.

Watson, M.G., Byrne, H.M., Macaskill, C., Myerscough, M.R., 2018. A two-phase model of early fibrous cap formation in atherosclerosis. *Journal of Theoretical Biology* 456, 123–136.

Watson, M.G., Byrne, H.M., Macaskill, C., Myerscough, M.R., 2020. A multiphase model of growth factor-regulated atherosclerotic cap formation. *Journal of Mathematical Biology* 81, 725–767.

Watson, M.G., Chambers, K.L., Myerscough, M.R., 2023. A lipid-structured model of atherosclerotic plaque macrophages with lipid-dependent kinetics. *Bulletin of Mathematical Biology* 85, 85.

Wu, M.Y., Li, C.J., Hou, M.F., Chu, P.Y., 2017. New insights into the role of inflammation in the pathogenesis of atherosclerosis. *International Journal of Molecular Sciences* 18, 2034.

Zaman, A., Ali, N., Bég, O.A., 2016. Unsteady magnetohydrodynamic blood flow in a porous-saturated overlapping stenotic artery—numerical modeling. *Journal of Mechanics in Medicine and Biology* 16, 1650049.

Zhang, K., Kaufman, R.J., 2003. Unfolding the toxicity of cholesterol. *Nature cell biology* 5, 769–770.

Zheng, C., Yang, Q., Cao, J., Xie, N., Liu, K., Shou, P., Qian, F., Wang, Y., Shi, Y., 2016. Local proliferation initiates macrophage accumulation in adipose tissue during obesity. *Cell death & disease* 7, e2167–e2167.